DEVELOPMENTAL BIOLOGY

Expression of the transcription factor Klf6 by thymic epithelial cells is required for thymus development

Justin Malin[1]†, Gustavo Ulises Martinez-Ruiz[1,2,3]†*, Yongge Zhao[1]†, Susannah C. Shissler[1], Jennifer E. Cowan[1,4], Yi Ding[1], Abigail Morales-Sanchez[1,3], Masaki Ishikawa[1,5], Marieke Lavaert[1], Arundhoti Das[1], Donna Butcher[6], Andrew C. Warner[6], Melissa Kallarakal[1], Jingqiu Chen[7,8], Noemi Kedei[7], Michael Kelly[9], Lauren R. Brinster[10], David Allman[5], Avinash Bhandoola[1]*

Thymic epithelial cells (TEC) control T cell development and play essential roles in establishing self-tolerance. By using *Foxn1-Cre*–driven ablation of *Klf6* gene in TEC, we identified *Klf6* as a critical factor in TEC development. *Klf6* deficiency resulted in a hypoplastic thymus—evident from fetal stages into adulthood—in which a dramatic increase in the frequency of apoptotic TEC was observed. Among cortical TEC (cTEC), a previously unreported cTEC population expressing the transcription factor Sox10 was relatively expanded. Within medullary TEC (mTEC), mTEC I and Tuft-like mTEC IV were disproportionately decreased. *Klf6* deficiency altered chromatin accessibility and affected TEC chromatin configuration. Consistent with these defects, naïve conventional T cells and invariant natural killer T cells were reduced in the spleen. Late stages of T cell receptor–dependent selection of thymocytes were affected, and mice exhibited autoimmunity. Thus, Klf6 has a prosurvival role and affects the development of specific TEC subsets contributing to thymic function.

INTRODUCTION

T cells are an essential component of the adaptive immune system that develops in the thymus. Distinct anatomical compartments in the thymus support sequential stages of T cell development. Multipotent progenitors migrating from bone marrow initially develop in the cortex, where cortical thymic epithelial cells (cTEC) regulate population expansion of early thymic progenitors, T cell lineage commitment, and rearrangement of the T cell receptor (TCR) (*1*, *2*). cTEC also present major histocompatibility complex (MHC)–peptide ligands for the positive selection of immature thymocytes, resulting in their maturation to $CD4^+$ or $CD8^+$ single-positive (SP) thymocytes. Selected thymocytes migrate to the medulla where they are exposed to tissue-restricted antigens (TRAs) on medullary TEC (mTEC). Thymocytes strongly recognizing TRAs are deleted or diverted into regulatory T (T_{reg}) cell lineage. In addition to conventional αβ T cells, the thymus also controls the development of several nonconventional T cell lineages, including γδ T cells, mucosal-associated invariant T cells, and invariant natural killer T (iNKT) cells (*2*, *3*).

Recent studies have greatly enhanced our knowledge of mTEC. Using flow cytometry, $mTEC^{lo}$ are defined by low surface expression levels of CD80 and MHC class II proteins, whereas $mTEC^{hi}$ express high surface levels of these proteins (*4*–*6*). Single-cell genomic technologies have further identified and characterized mTEC subpopulations. Most $mTEC^{hi}$ correspond to mTEC II, expressing *Aire* and high levels of MHC class II molecules, as well as TRA (*7*). $mTEC^{lo}$ contain multiple subsets: among these populations, mTEC I express *Itga6*, *Sca1*, and *Ccl21a* (*7*); mTEC III were initially identified by *Ly6d* and *Pigr* gene expression (*7*) but are now recognized to transcriptionally and epigenetically mimic a broad range of peripheral tissue cell types (*8*, *9*); and mTEC IV bear a transcriptional profile resembling peripheral gut tuft cells and require the transcription factor Pou2f3 (*7*, *10*).

mTEC I express high levels of the *Ccl21a* gene, which encodes the chemokine CCL21. CCL21 mediates thymic medullary recruitment of positively selected thymocytes through their CCR7 receptor (*11*). *Ccl21a* deficiency leads to autoimmune phenotypes resulting from the defective establishment of central tolerance in the thymic medulla (*11*, *12*). Besides their role in conventional T cell development, mTEC I also mediate iNKT development. Conditional ablation of the *Ltbr* gene in TEC resulted in reduced numbers of $CCL21^+CD104^+$ $mTEC^{lo}$ (mTEC I) and $CCL21^-CD104^-DCLK1^+$ $mTEC^{lo}$ (mTEC IV) (*3*). These intrathymic defects reduced peripheral iNKT cell pools (*3*). While the importance of mTEC I is functionally recognized, transcriptional regulators important for their development and function have not been identified.

Krüppel-like factor 6 (Klf6) is a transcription factor that is broadly expressed (*13*), and its aberrant expression is implicated in multiple cancers (*14*, *15*). Germline mutation of *Klf6* is embryonically lethal (*16*), highlighting its nonredundant functions; and its conditional ablation affected differentiation and survival of prostate epithelial cells (*17*). In the present study, we investigated the role of the *Klf6* gene in thymus development and function through in vivo ablation in TEC by crossing mice with conditional alleles of *Klf6* to

[1]Laboratory of Genome Integrity, Center for Cancer Research, National Cancer Institute, National Institutes of Health, Bethesda, MD, USA. [2]Research Division, Faculty of Medicine, National Autonomous University of Mexico, Mexico City, Mexico. [3]Children's Hospital Federico Gomez, Mexico City, Mexico. [4]Institute of Immunity and Transplantation, University College London, London, UK. [5]Department of Pathology and Laboratory Medicine, Perelman School of Medicine at the University of Pennsylvania, Philadelphia, PA, USA. [6]Molecular Histopathology Laboratory, Frederick National Laboratory for Cancer Research, Frederick, MD, USA. [7]Office of Science and Technology Resources, Center for Cancer Research, National Cancer Institute, National Institutes of Health, Bethesda, MD, USA. [8]ACROBiosystems, Newark, DE, USA. [9]Single Cell Analysis Facility, Center for Cancer Research, National Cancer Institute, National Institutes of Health, Bethesda, MD, USA. [10]Division of Veterinary Resources, Office of Research Services, National Institutes of Health, Bethesda, MD, USA.
*Corresponding author. Email: avinash.bhandoola@nih.gov (A.B.); ulises.mtzruiz@facmed.unam.mx (G.U.M.-R.)
†These authors contributed equally to this work.

mice expressing Foxn1-Cre. We report that *Klf6* deficiency in TEC resulted in thymic hypoplasia beginning from prenatal life and extending through adulthood. Guided by single-cell transcriptional profiling, we determined that loss of *Klf6* increased programmed cell death of TEC in prenatal and adult mice. In adult mice, *Klf6* deficiency severely affected the differentiation of the mTEC I and mTEC IV populations. In addition, *Klf6* deficiency led to the relative expansion of a previously uncharacterized cTEC population expressing *Sox10* that is present in wild-type mice at very low frequencies. We observed concordant reductions of the naïve αβ T cell and iNKT pools in the periphery of young adult mice. Furthermore, we detected T cell infiltration in salivary and lacrimal glands and increased titers of anti–double-stranded DNA (dsDNA) autoantibodies, consistent with defects in T cell tolerance.

The present study thus establishes that the transcription factor Klf6 is critical for TEC development and regulates mTEC I and mTEC IV differentiation. Thus, *Klf6* expression by TEC is essential for normal thymic function and the establishment of self-tolerance.

RESULTS

Conditional knockout of the Klf6 gene compromises thymus development

We examined expression levels of *Klf6* in TEC a multiple age points, using previously published bulk RNA sequencing (RNA-seq) (*18*). We observed an expression that appeared comparable to well-known regulators of TEC such as Foxn1 (*19*) and p63 (fig. S1A) (*20*). To test the role of Klf6 in TEC, we bred mice to lack *Klf6* specifically in TEC. *Foxn1-Cre* mice were crossed with mice in which loxP sites flanked exons 2 and 3 of the *Klf6* locus (*17*). We refer to these *Foxn1-Cre*$^{+}$ *Klf6*$^{fl/fl}$ mice as "Klf6^{KO}." Loss of Klf6 protein in mTEC was confirmed by a Simple Western capillary electrophoresis assay, comparing samples from 4-week-old Klf6^{KO} to littermate controls (*Foxn1-Cre*$^{-/-}$; *Klf6*$^{fl/fl}$, referred to as "Klf6^{WT}") (fig. S1B). As Klf6 expression was unaltered in both thymocytes and splenocytes from Klf6^{WT} and Klf6^{KO} mice (fig. S1C), *Foxn1*-mediated Klf6 protein loss was specific for TEC in the thymus.

As early as embryonic day (E) 14.5, the thymus was smaller in Klf6^{KO} relative to Klf6^{WT} mice and remained smaller at all later ages that we assessed (Fig. 1, A and B). Particularly after birth, the thymus consists overwhelmingly of thymocytes, with their number and development controlled by TEC (*6*, *18*). Lymphocyte cellularity was markedly reduced in the Klf6^{KO} thymus. We determined the frequency of early T cell progenitors but observed minimal alterations, indicating that recruitment of lymphoid precursors to the thymus was not severely affected (fig. S1D) (*21*). Whereas CD4^{+} and CD8^{+} SP thymocyte subset frequencies were not affected (Fig. 1C and fig. S1, E and G), the absolute numbers of these populations were reduced (fig. S1, F and H). CD4^{+} T_{reg} cells and their precursors (*22*) were similarly proportionally represented but reduced in number (fig. S1, I and J). TEC were identified on the basis of flow cytometry as CD45^{-}EpCAM^{+} and quantitated at E15.5, E17.5, 7 days, and 4 weeks of age. Consistent with the smaller thymus in Klf6^{KO} mice, numbers of TEC were reduced in the absence of Klf6 (Fig. 1D and fig. S1K) at all time points evaluated. The expression of KLF6 mRNA was also evident in TEC populations isolated from humans (fig. S1, L and M). These data indicate that *Klf6* is expressed in mouse and human TEC and is required for normal mouse thymus development.

Klf6-deficient mice exhibit decreased numbers of cTEC and mTEC

Since we observed decreased thymus size and TEC cellularity in Klf6^{KO} mice starting from E14.5 and extending through adulthood, we asked whether cTEC (CD45^{-}EpCAM^{+}Ly51^{+}UEA1^{-}) and mTEC (CD45^{-}EpCAM^{+}Ly51^{-}UEA1^{+}) were affected uniformly. We quantified cTEC and mTEC at E15.5, E17.5, 7 days, and 4 weeks of age (Fig. 2A). cTEC and mTEC were reduced in Klf6^{KO} at all time points (Fig. 2, A to C). *Klf6* loss resulted in a consistently larger defect in mTEC than in cTEC, with the highest deficit occurring at 4 weeks of age (Fig. 2, B and C). mTEC are subdivided into two broad compartments, mTEC^{lo} (MHCII^{lo}CD80^{lo}) and mTEC^{hi} (MHCII^{high}CD80^{high}). Therefore, we characterized the impact of Klf6 deficiency in mTEC^{lo} and mTEC^{hi} compartments at E17.5 and postnatally at 1 and 4 weeks (fig. S2A). As expected, dramatic reductions in total cell numbers in mTEC^{lo} and mTEC^{hi} were evident across the analyzed ages (Fig. 2D). Changes in the frequency of these compartments were maximal at 4 weeks of age, resulting in an evident reduction of mTEC^{lo} (fig. S2B). In Klf6^{KO} mice, the overall thymus size and total number of cells were reduced with an increased cortex:medulla ratio by hematoxylin and eosin (H&E) staining (fig. S2, C to E). Klf6^{KO} medullary areas remained distinct, showing no gross defects in structure and with the appropriate expression of medullary-specific markers (UEA1, CCL21, and Aire) assessed by confocal microscopy (Fig. 2E and fig. S2D). The marked reduction in mTEC cellularity emphasizes the importance of *Klf6* in mTEC development.

Embryonic Klf6^{KO}-specific cluster up-regulated apoptosis-associated genes

Impaired thymic growth was evident in fetal Klf6^{KO} mice (Fig. 1). To better understand the requirement for *Klf6* in TEC, cell-sorted TEC from E15.5 Klf6^{KO} and Klf6^{WT} mice were submitted for parallel single-cell RNA-seq (scRNA-seq) using the 10x Genomics Chromium platform. The two scRNA-seq datasets were integrated and projected into a two-dimensional Uniform Manifold Approximation and Projection (UMAP) (Fig. 3A and fig. S3A), where we applied an annotation strategy using previously published marker genes (*7*). cTEC expressed *Cxc12* and *Psmb11* (fig. S3A) and contained the majority of cells (Fig. 3, A and B). mTEC II were identified on the basis of the expression of *Aire* and *Fezf2* (fig. S3A) (*7*). In addition, we observed a cluster of cells expressing the *Sox10* gene (fig. S3A), which will be further described later. We did not find clusters with a substantial expression of gene markers associated with either mTEC III or mTEC IV. One cluster exhibited expression of genes without previously validated function in TEC such as *Rab25*, *Spink8*, and *Tacstd2* (fig. S3A). This cluster is labeled "eTEC" for embryonic TEC (Fig. 3A and fig. S3A) of uncertain provenance, which have been previously observed (*7*, *23*).

There was a large subset of E15.5 Klf6^{KO} TEC that aligned poorly with E15.5 Klf6^{WT} TEC (Fig. 3A). To isolate this subset, we calculated clusters across the integrated Klf6^{WT}-Klf6^{KO} dataset, choosing the resolution for which the Klf6^{KO}-specific subset mapped as a single cluster (Fig. 3C). This cluster, labeled "Klf6^{KO}-specific cluster", contained 35% of the cells in Klf6^{KO} dataset and 97% were annotated as cTEC (Fig. 3, D and E). In the integrated Klf6^{WT}-Klf6^{KO} UMAP, the Klf6^{KO}-specific cluster contained just 12 Klf6^{WT} cells that shared the transcriptional signature of 1454 Klf6^{KO} cells (Fig. 3C, left).

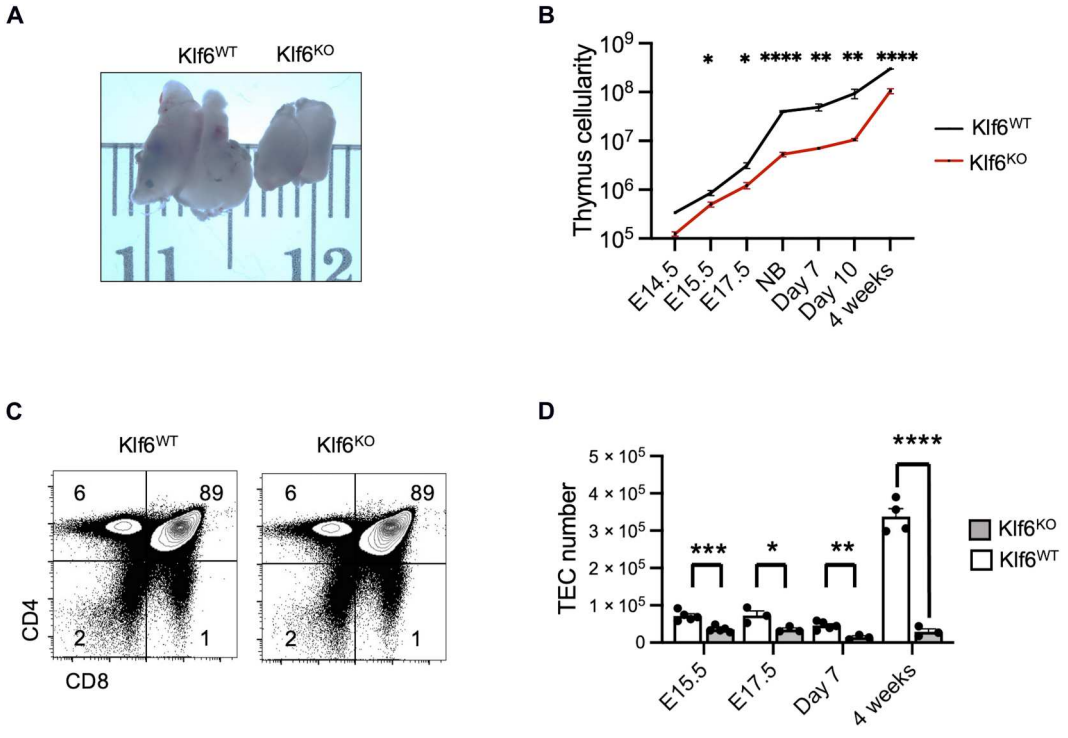

Fig. 1. Conditional deletion of Klf6 in TEC reduced thymic growth and TEC cellularity. (**A**) Photograph of 4-week-old thymi from Klf6^{WT} (left) and Klf6^{KO} (right) mice. The included ruler has major ticks every 1 cm, and minor ticks every 1 mm. (**B**) Total thymus cell counts from embryonic (E) to adult ages for Klf6^{WT} (black) and Klf6^{KO} (red) mice. NB, newborn. (**C**) Representative flow cytometric plots of CD4 versus CD8 profiles in thymus. Plots are gated on live singlet cells. (**D**) TEC cellularity from embryonic (E) to adult ages for Klf6^{WT} (white) and Klf6^{KO} (gray) mice. (B and D) Significance computed using two-tailed unpaired Student's *t* tests. Error bars show ±1 SEM for a minimum of *n* = 3 mice per age. (B to D) Data are representative of or include at least four independent experiments.

To better characterize the Klf6^{KO}-specific cluster, we identified the differentially expressed genes (DEGs) up-regulated in the Klf6^{KO}-specific cluster compared with Klf6^{WT} cells (Fig. 3C) and used them for Gene Ontology (GO) pathway analysis. Apoptosis and stress-related pathways were enriched in the Klf6^{KO}-specific cluster (Fig. 3F). GO pathway analyses were also performed on DEG up-regulated in Klf6^{WT} compared to Klf6^{KO} TEC, not including the Klf6^{KO}-specific cluster. We observed enrichment in terms associated with resistance to apoptosis in the Klf6^{WT} TEC (Fig. 3G). Consistently, up-regulation of apoptosis and stress-related genes was observed in all Klf6^{KO} TEC, including the Klf6^{KO}-specific cluster (Fig. 3H). These trends were confirmed on sorted E15.5 TEC via reverse transcription quantitative polymerase chain reaction (RT-qPCR) of the *Pmaip1* gene, encoding Noxa which represses Bcl-2 proteins, allowing intrinsic apoptotic activation; and the *Cdkn1a* gene, which is associated with both stress-induced cell cycle arrest and apoptosis through either p53-dependent or p53-independent pathways (Fig. 3I) (*24*).

Elevated apoptosis in fetal TEC lacking Klf6 gene expression

To determine whether enhanced apoptotic gene signature corresponded with increased apoptosis, we performed in situ immunofluorescence and terminal deoxynucleotidyl transferase–mediated deoxyuridine triphosphate nick end labeling (TUNEL) staining on E15.5 embryos. TEC nuclei were stained for p63, a marker of epithelial cells (Fig. 3J) (*20*, *25*). The fraction of p63^{+} cells co-stained with TUNEL was eightfold higher in Klf6^{KO} than in Klf6^{WT} fetal TEC (Fig. 3K). Because there is no previous report assessing potential genotoxicity mediated by expression of the *Foxn1-Cre* transgene itself, and other Cre mouse lines can exhibit genotoxicity (*26*), we also assessed the thymus of E15.5 embryos expressing only the *Foxn1-Cre* transgene. There was no change in the TUNEL^{+} TEC frequency of thymi from *Foxn1-Cre* embryos compared with wild-type and Klf6^{WT} embryos (Fig. 3K). We did not observe differences in total thymic cellularity or the expression of *Pmaip1* and *Cdkn1a* genes between *Foxn1-Cre* versus Klf6^{WT} embryos (Fig. 3I). Thus, we conclude that the observed results were due to deficiency of *Klf6* rather than expression of *Foxn1-Cre* by itself. To resolve apoptosis within cTEC and mTEC subsets in E15.5 mice, we stained for cleaved caspase-3 by flow cytometry. The proportion of cleaved caspase-3^{+} cells in Klf6^{KO} compared to Klf6^{WT} was fivefold higher in cTEC and more than ninefold in mTEC (Fig. 3L and fig. S3C). In concordance with the cross-talk between thymocytes and TEC (*27*, *28*), there was also a significant difference of ~2-fold in CD45^{+} thymocytes (fig. S3B). These results provide strong evidence for elevated apoptosis in E15.5 Klf6^{KO} TEC.

Some DEGs were associated with both apoptosis and cell cycle regulation, such as *Cdkn1a*, suggesting reduced proliferation in E15.5 Klf6^{KO} TEC. To assess proliferation, we performed in vivo bromodeoxyuridine (BrdU) labeling. The frequency of E15.5 TEC that incorporated BdrU 18 hours after administration was not altered (fig. S3, D and E). In summary, the increased apoptosis

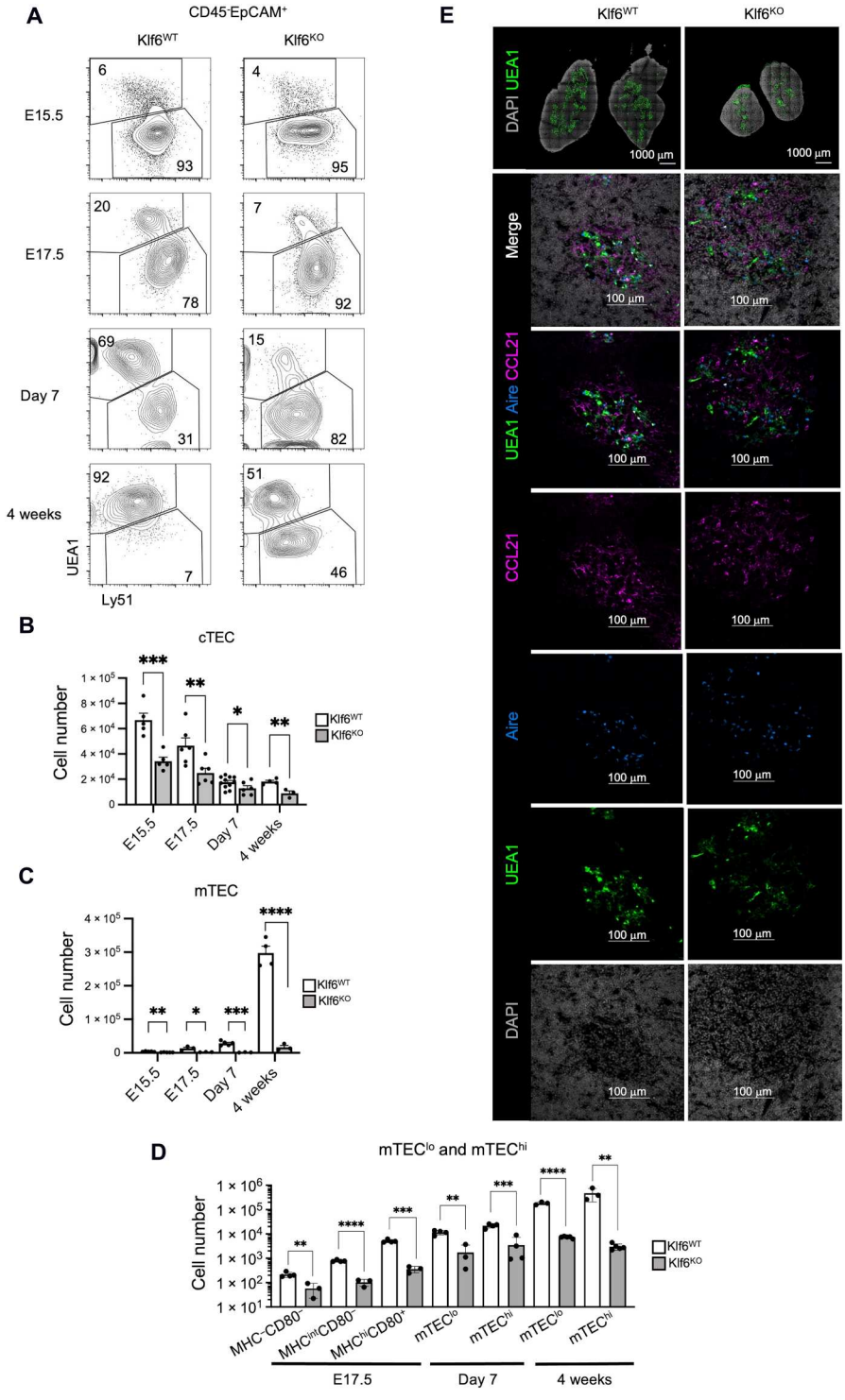

Fig. 2. Klf6^{KO} thymi had a greatly reduced mTEC compartment. (**A**) Representative flow cytometric plots of the frequency of Ly51^{+} UEA1^{-} cTEC and Ly51^{-} UEA1^{+} mTEC from embryonic to adult ages for Klf6^{WT} (left) and Klf6^{KO} (right) mice. Plots are gated for live, singlet, CD45^{-} EpCAM^{+} TEC. (**B** and **C**) Cell counts of cTEC (B) and mTEC (C) from Klf6^{WT} (white) and Klf6^{KO} (gray) mice at the same ages as in (A), shown as barplots. (**D**) mTEC^{lo} (MHCII^{lo}CD80^{lo}) and mTEC^{hi} (MHCII^{high}CD80^{high}) number. For embryonic TEC at day 17.5 of gestation, subsets include an additional MHCII^{int}CD80^{-} population as previously published (*50*). (**E**) Confocal images of Klf6^{WT} (left) and Klf6^{KO} (right) thymus with staining for 4′,6-diamidino-2-phenylindole (DAPI) and antibodies specific for UEAI, Aire, and CCL21. Three Klf6^{WT} and five Klf6^{KO} thymi were examined. (A to D) Data are representative of or include a minimum of two and usually four or more independent experiments. Significance was computed using two-tailed unpaired Student's *t* tests. Error bars are +1 SEM with a minimum of $n = 3$ mice per age.

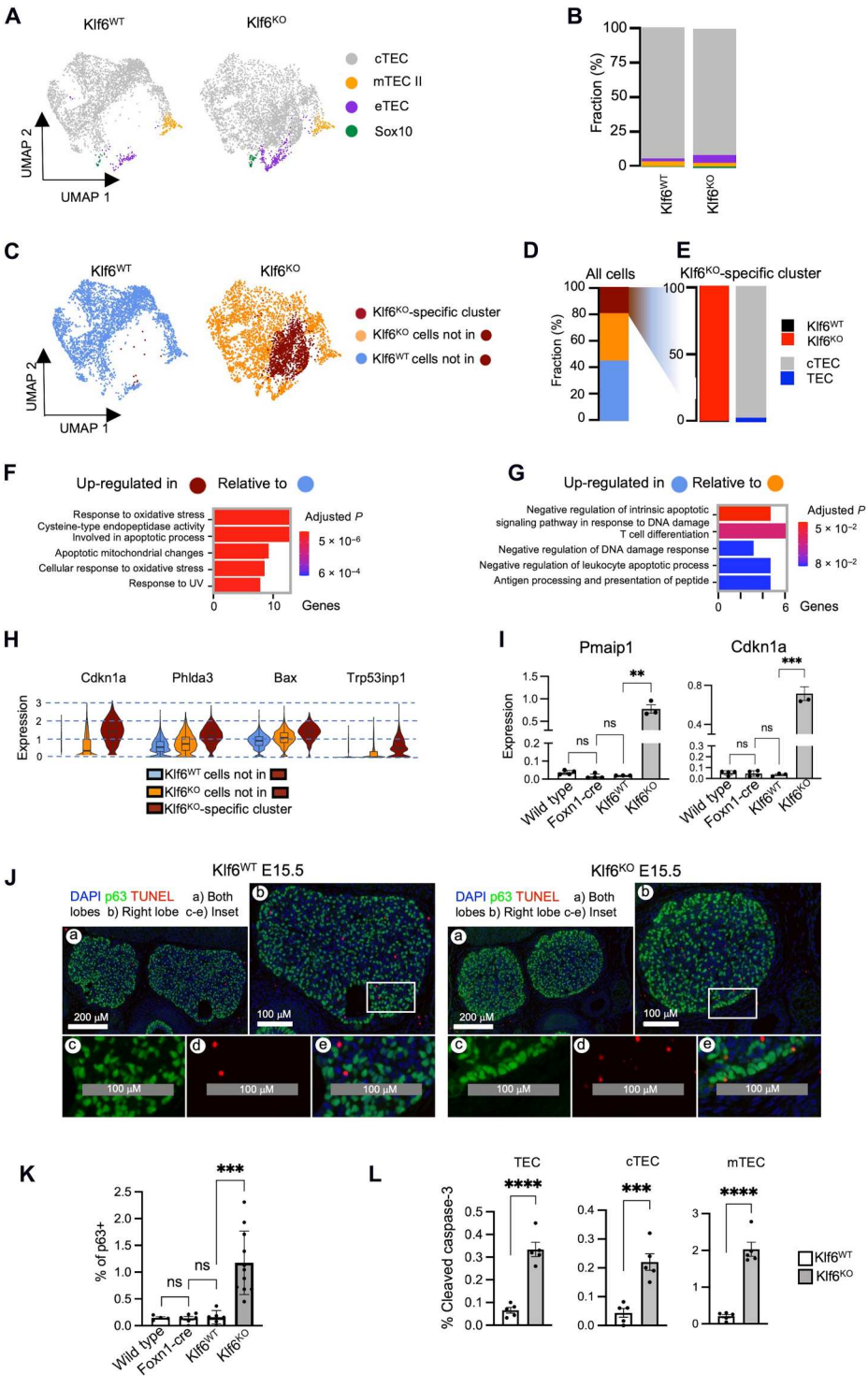

Fig. 3. Elevated apoptosis in fetal Klf6^{KO} TEC. (**A**) UMAP of scRNA-seq data for 3511 Klf6^{WT} (left) and 4136 Klf6^{KO} (right) sorted E15.5 whole TEC (CD45$^-$EpCAM$^+$). Clusters are colored by the TEC subset (see legend). (**B**) Stacked barplot showing relative frequencies of clusters from (A). (**C**) UMAP showing three clusters of Klf6^{WT} and Klf6^{KO} cells: Klf6^{KO}-specific (dark red), Klf6^{KO} cells not in the Klf6^{KO}-specific cluster (orange), and Klf6^{WT} cells not in the Klf6^{KO}-specific cluster (cyan). (**D**) Stacked barplot showing frequencies of clusters from (C). (**E**) Stacked barplot showing frequencies of Klf6^{KO}-specific cluster broken down by Klf6^{WT}/Klf6^{KO} samples and cTEC versus other TEC (mTECII, eTAC, and Sox10) clusters. (**F**). Gene Ontology (GO) pathway analysis for genes up-regulated in Klf6^{KO}-specific cluster compared with Klf6^{WT} TEC not included in the Klf6^{KO}-specific cluster, *P* value adjusted by Benjamini-Hochberg procedure. (**G**) GO pathway analysis of DEG up-regulated in Klf6^{WT} cluster compared with Klf6^{KO} cluster excluding Klf6^{KO}-specific cluster, *P* value adjusted by Benjamini-Hochberg procedure. (**H**) Violin plots of select genes up-regulated in Klf6^{KO}-specific cluster associated with enriched GO terms from (F). (**I**) Barplots of *Pmaip1* and *Cdkn1a* gene expression measured by reverse transcription quantitative polymerase chain reaction assays of sorted E15.5 TEC from wild-type, *Foxn1*:*Cre*$^+$, Klf6^{WT}, and Klf6^{KO} embryos. The data represent at least three mice per group. (**J**) Terminal deoxynucleotidyl transferase–mediated deoxyuridine triphosphate nick end labeling (TUNEL) immunofluorescence of E15.5 thymus from Klf6^{WT} (left) and Klf6^{KO} (right) including DAPI, p63 (TEC nuclei), and TUNEL (apoptotic cells, orange-red); representative of at least three mice per group. (**K**) Barplot of the proportion of TUNEL$^+$ nuclei within p63$^+$ nuclei from E15.5 thymi from wild-type, *Foxn1-Cre*$^+$, Klf6^{WT}, or Klf6^{KO} embryos. (**L**) Barplots of the proportion of cleaved caspase-3$^+$ cells in whole TEC (CD45$^-$EpCAM$^+$), cTEC (Ly51$^+$UEAI$^-$), or mTEC (Ly51$^-$UEAI$^+$) from Klf6^{WT} (white) and Klf6^{KO} (gray) embryos. Error bars show ±1 SEM for $n \geq 5$ mice per group. The data are representative of at least three independent experiments. ns, not significant.

observed in E15.5 Klf6^{KO} TEC indicates that *Klf6* has a prosurvival role in TEC.

Loss of Klf6 compromises mTEC I and mTEC IV compartments

Given the dramatic reduction observed in the mTEC compartment of 4-week-old Klf6^{KO} mice (Fig. 2, A to D) and the expansion of multiple mTEC subsets postnatally, we sought to determine whether *Klf6* ablation affects specific mTEC subsets. To address this question, we transcriptionally profiled TEC in 4-week-old Klf6^{KO} and Klf6^{WT} mice using scRNA-seq.

A total of seven TEC clusters were identified in the integrated adult Klf6^{WT} and Klf6^{KO} data by using well-known marker genes (Fig. 4A and fig. S4A) (*7*). We identified a cTEC cluster, which

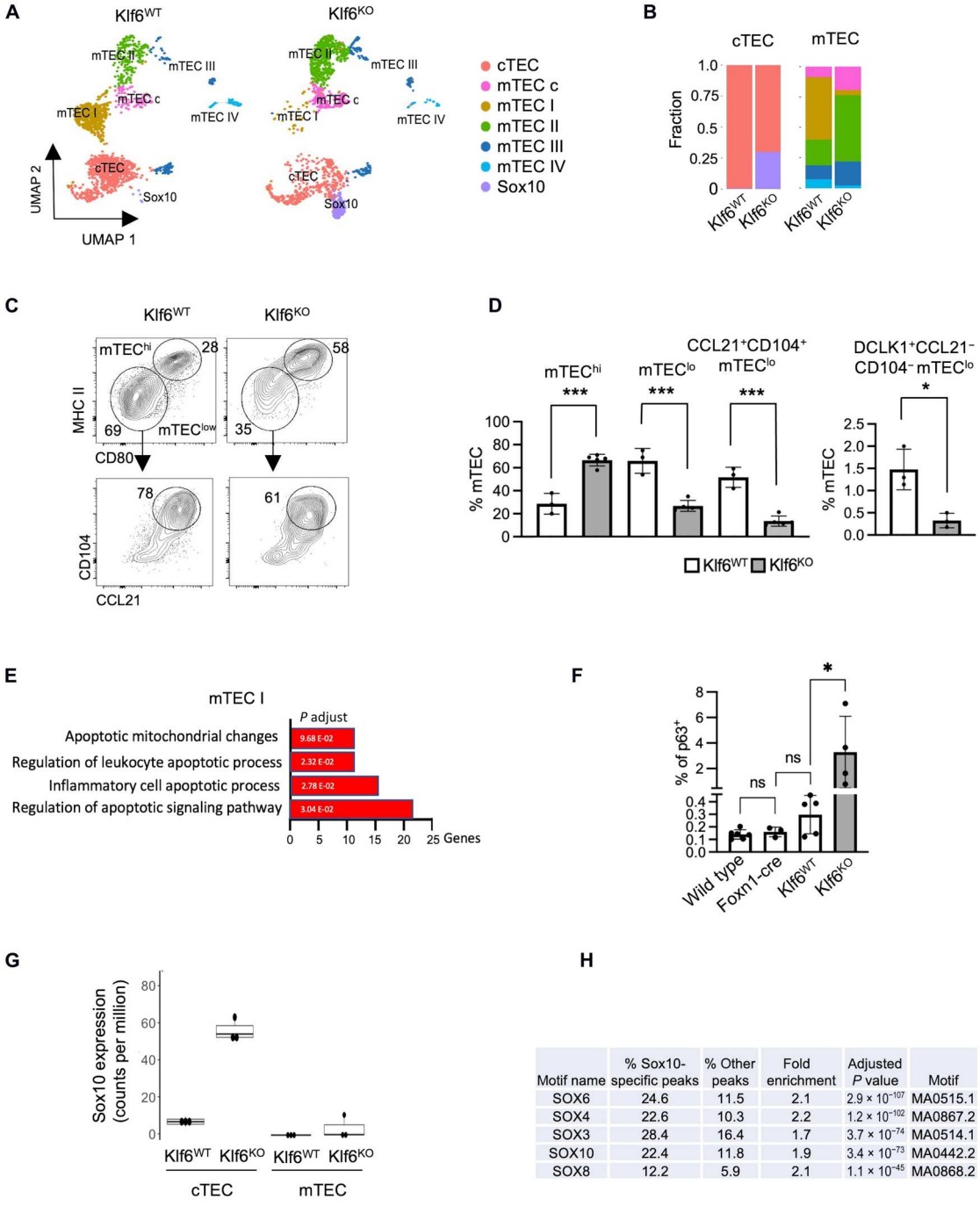

H

Motif name	% Sox10-specific peaks	% Other peaks	Fold enrichment	Adjusted *P* value	Motif
SOX6	24.6	11.5	2.1	2.9×10^{-107}	MA0515.1
SOX4	22.6	10.3	2.2	1.2×10^{-102}	MA0867.2
SOX3	28.4	16.4	1.7	3.7×10^{-74}	MA0514.1
SOX10	22.4	11.8	1.9	3.4×10^{-73}	MA0442.2
SOX8	12.2	5.9	2.1	1.1×10^{-45}	MA0868.2

Fig. 4. In adult Klf6^{KO} thymi, mTEC I were severely depleted, whereas a Sox10-expressing cTEC cluster expanded. (**A**) UMAP of scRNA-seq data for 1762 Klf6^{WT} (left) and 1593 Klf6^{KO} (right) TEC sorted from 4-week-old mice. Clusters are colored by the TEC subset (see legend). (**B**) Stacked barplot of relative proportions of cTEC and mTEC clusters shown in (A), calculated as a proportion of total cTEC or total mTEC, respectively. (**C**) Representative flow cytometry plot of the frequency of mTEC^{lo} (MHC II^{lo}CD80^{lo}) and mTEC^{hi} (MHC II^{high}CD80^{high}) gated on live singlet mTEC. From the mTEC^{lo}, mTEC I were identified as CD104^{+}CCL21^{+} in the Klf6^{WT} (left) and Klf6^{KO} (right) samples. The data are representative of four independent experiments. (**D**) Corresponding barplots of the relative frequencies of mTEC^{hi}, mTEC^{lo}, CD104^{+}CCL21^{+} mTEC^{lo}, and CD104^{-}CCL21^{-}DCLK1^{+} mTEC^{lo} within mTEC from Klf6^{WT} (white) and Klf6^{KO} (gray) mice. Data are representative of four independent experiments. (**E**) GO pathway analysis for genes up-regulated in Klf6^{KO} mTEC I compared with Klf6^{WT} mTEC I. *P* value adjusted by Benjamini-Hochberg procedure. (**F**) Barplot of the proportion of TUNEL^{+} nuclei (apoptotic cells) within p63^{+} nuclei (TEC) from immunofluorescence staining of thymus from 4-week-old wild-type, *Foxn1-Cre*$^{+}$, Klf6^{WT}, and Klf6^{KO} mice. Statistical significance for barplots was computed using a two-tailed unpaired Student's *t* test. The data are representative of at least three mice in each group. (**G**) *Sox10* expression from bulk RNA-seq of sorted cTEC (CD45^{-}EpCAM^{+}Ly51^{+}UEA1^{-}) and mTEC (CD45^{-}EpCAM^{+}Ly51^{-}UEA1^{+}) from 4-week-old Klf6^{KO} and Klf6^{WT} mice. Shown are the mean (horizontal line) and 95% confidence intervals (box) for $N = 3$ samples. (**H**) Top enriched motifs in differentially accessible chromatin of the Sox10 cluster calculated using Signac and scATAC-seq (single-cell assays for transposase-accessible chromatin using sequencing) data from 4-week-old Klf6^{WT} and Klf6^{KO} mice. Significance was computed using two-tailed unpaired Student's *t* tests. Error bars show ±1 SEM for a minimum of $n = 3$ mice per age.

expressed *Cxcl12* and *Psmb11*; an mTEC I cluster, based on differential expression of *Ccl21a* and *Itgb4 (3)*; a cluster of mTEC II, based on *Aire* and *Fezf2*; a cluster of mTEC III, based on *Ly6d* and *Ivl*; an mTEC IV cluster which expressed *Pou2f3* and *Il25* and resembles intestinal Tuft cells (*7*, *10*); an mTECc cluster which expressed cell cycle genes and specific chromatin-associated genes observed in prior studies (*29*, *30*); and lastly, a *Sox10*-expressing cTEC subset that will be discussed later. DEGs (table S1) and GO pathway analyses from both up-regulated and down-regulated DEG were compiled for each TEC population (table S2).

We next examined the proportions of mTEC subpopulations in Klf6^{KO} (Fig. 4B). We found that the proportions of mTEC II and mTEC III increased modestly in the Klf6^{KO} (2.8-fold and 1.9-fold, respectively), whereas the proportions of mTEC I and mTEC IV fell (12.2-fold and 2.9-fold, respectively).

The differences observed at the single-cell level in the Klf6^{KO} were corroborated by flow cytometry (Fig. 4C). In concordance with the increase in mTEC II observed at the single-cell level (Fig. 4, A and B), the proportion of mTEC^{hi} was significantly higher while the mTEC^{lo} fraction was decreased in the Klf6^{KO} compared with the Klf6^{WT} thymus (Fig. 4D). Within the mTEC^{lo} compartment (*3*), alterations in mTEC I and mTEC IV were considered to correspond to CCL21^{+}CD104^{+} and CCL21^{-}CD104^{-}DCLK1^{+} mTEC^{lo}, respectively (Fig. 4, C and D), as previously reported (*3*). As expected, mTEC I were decreased at least fourfold and mTEC IV were reduced fivefold in the Klf6^{KO} compared with the Klf6^{WT} thymus (Fig. 4D). *Klf6* deficiency in mTEC IV did not alter *Pou2f3* gene expression levels (fig. S4B). Thus, although Klf6 influences the development of all mTEC subsets, it is notably required for mTEC I and mTEC IV subpopulations.

mTEC I undergo apoptosis in Klf6^{KO} mice

CCL21^{+}CD104^{+} mTEC^{lo} (mTEC I) were the most affected major population in the Klf6^{KO} mice. Among the major mTEC populations, *Klf6* expression was higher in mTEC I compared to mTEC II in mice (fig. S4C) and also in humans (fig. S1M). The average expression of *Ccl21a* was modestly reduced in Klf6^{KO} mice (fig. S4D, left), but CCL21 protein levels were not changed in the remaining CCL21^{+}CD104^{+} mTEC^{lo} (fig. S4D, right). The observed reduction in the frequencies of CCL21^{+}CD104^{+} and CCL21^{-}CD104^{-}DCLK1^{+} mTEC^{lo} with no decrease in CCL21 protein expression is reminiscent of mice lacking *Ltbr* in TEC (LTβR^{KO}) (*3*), but no reduction in *Ltbr* expression, or surface expression of Ltbr, was evident in Klf6^{KO} mTEC I (fig. S4, E and F). Therefore, we sought other explanations of the observed phenotype in Klf6^{KO} mice.

GO pathway analyses on mTEC I up-regulated DEG in the Klf6^{KO} compared with Klf6^{WT} (Fig. 4E) were enriched for apoptosis-related pathways that were also present when all Klf6^{KO} TEC were compared with the Klf6^{WT} TEC (fig. S4G). As background levels of caspase-3 activation and annexin V staining are high in adult TEC due to digestion preparations (*5*), we evaluated apoptosis by performing TUNEL staining in situ on 4-week-old thymi. As with E15.5 mice, co-staining for p63 and TUNEL was quantified. We observed a 15-fold higher frequency of TUNEL^{+} TEC in Klf6^{KO} than in Klf6^{WT} (Fig. 4F). Therefore, apoptosis was elevated in embryonic and adult Klf6^{KO} TEC. We did not observe any difference in the TUNEL^{+} TEC frequency or total thymic cellularity comparing thymi from *Foxn1-Cre* with Klf6^{WT} or wild-type mice (Fig. 4F and fig. S2C), confirming that the observed results reflected a requirement for Klf6 in TEC.

Immediate precursors of Aire^{+} and CCL21^{+} mTEC are contained in a population of proliferative adult mTEC (*5*, *29*, *30*), corresponding to the mTECc cluster (Fig. 4A). Cell cycle scores from the mTECc cluster in the Klf6^{WT} and Klf6^{KO} revealed no differences (fig. S4H). To assess proliferation experimentally, in vivo BrdU labeling was performed on 4-week-old mice. Whereas no alteration in the frequency of BrdU incorporation into thymocytes or mTEC^{hi} was observed, the frequency of BrdU^{+} total mTEC and CCL21^{+}CD104^{+} mTEC^{lo} was significantly increased in Klf6^{KO} compared to Klf6^{WT} thymus (fig. S4I), and, as expected, all Klf6^{KO} TEC subsets were numerically reduced (fig. S4J). The increment in the frequency of proliferating mTEC I in Klf6^{KO} might result from an absence of the most differentiated nonproliferative cells. To assess mTEC I differentiation, we reclustered only mTECc, mTEC I, and mTEC II and performed pseudo-time analysis using Monocle3. On the basis of a previous report (*30*), the mTECc cluster was specified as a starting point to analyze the developmental trajectory of mTEC I and mTEC II (fig. S4, K to M, left). Using a gene signature score of mTEC I through cells ordered in pseudo-time, we found that Klf6^{KO} mTEC I lagged behind Klf6^{WT} mTEC I in this developmental trajectory (fig. S4M, middle). Conversely, mTEC II from Klf6^{KO} and Klf6^{WT} mice showed comparable transcriptional scores during their inferred developmental trajectories (fig. S4M, right). Combined, these data indicate that the reduction of the mTEC I compartment in Klf6^{KO} is due to increased apoptosis and reduced differentiation of surviving cells.

A Sox10-expressing TEC population is expanded in the thymus of Klf6^{KO} mice

Unexpectedly, we detected a cluster of cells in both our fetal and adult scRNA-seq datasets that expressed *Sox10* in a highly cluster-specific manner (figs. S3A and S4A); we refer to them as Sox10 TEC (Figs. 3A and 4A). This TEC cluster in E15.5 Klf6^{KO} and Klf6^{WT} embryos accounted for ~1 and 0.5% of TEC, respectively (Fig. 3B). In adult samples, Sox10 TEC frequency, calculated as the percentage of total cTEC, increased markedly from <1% (5 cells) in Klf6^{WT} to 29% (194 cells) in Klf6^{KO} (Fig. 4B).

Whereas Sox10 TEC were positioned contiguously with cTEC on the UMAP (Fig. 4A), we were unsure whether they segregate into the mTEC or cTEC compartments. Therefore, we sorted mTEC and cTEC from Klf6^{KO} and Klf6^{WT} for bulk RNA-seq (fig. S5A). *Sox10* expression was highest in the cTEC compartment (Fig. 4G). We compared Sox10 TEC from Klf6^{KO} and Klf6^{WT} thymi with mTEC and cTEC of Klf6^{KO} and Klf6^{WT} thymi, using our scRNA-seq datasets. *Ctsl* and *Krt8* were expressed robustly in Sox10 TEC, but *Psmb11*, *Cxcl12*, *Prss16*, and *Ly75* were lowly expressed (fig. S5B) (*7*). GO pathway analysis of DEG comparing the Klf6^{KO} Sox10 cluster with Klf6^{WT} TEC (up-regulated and down-regulated) identified pathways governing cell morphology, cell-cell junction assembly, and cell adhesion (fig. S5C). Furthermore, we inspected our scRNA-seq data to determine DEG in Sox10 TEC compared with wild-type cTEC (table S1). We performed GO analyses using the above DEG and observed enrichment in pathways linked to gland development, and again noted that Sox10 TEC expressed lower levels of genes involved in cell adhesion (fig. S5D). Overall, this is in concordance with the role of Sox10 as a transcription factor implicated in embryonic development (*31*).

In contrast to a previous report characterizing *Sox10*-expressing neural crest–derived cells present in the thymus as EpCAM$^-$ (*32*), our Sox10 TEC were sorted as EpCAM$^+$ and expressed higher EpCAM mRNA than other TEC populations (fig. S5B). We compared our population to a recently identified human myelin$^+$ TEC population, expressing *Sox10*, *Mbp*, and *Mpz* (*9*), but *Mbp* and *Mpz* expression was not Sox10-cluster specific in our dataset (fig. S5E).

To further characterize the Sox10 TEC population, we generated single-cell assays for transposase-accessible chromatin using sequencing (scATAC-seq) data from adult Klf6^{KO} and Klf6^{WT} TEC, described in the subsequent sections. Open chromatin regions present only in Sox10 TEC were significantly enriched for the Sox10 transcription factor motif and other Sox family motifs (Fig. 4H).

In summary, we identified a TEC subpopulation expressing *Sox10*, detectable only at very low frequencies in embryonic and adult Klf6^{WT} mice. Since ablation of *Klf6* relatively expands this population, increasing its frequency, Klf6 might negatively control the development of Sox10 TEC. Further research is needed to address the role of Klf6 in Sox10 TEC and its possible function.

Klf6^{KO} mice had reduced naïve conventional T cells and iNKT cells as well as autoimmunity

Peripheral lymphocyte pools were assessed in isolated splenocytes from 4- to 6-week-old Klf6^{KO} and Klf6^{WT} mice (fig. S6A). Cell counts did not vary between Klf6^{WT} and Klf6^{KO} for splenocytes nor for the CD19$^+$ B cell fraction (fig. S6, B and C). However, both CD4$^+$ and CD8$^+$ T cell counts were significantly decreased in Klf6^{KO} (Fig. 5, A and B). Within CD4$^+$ T cells, T_{reg} counts were minimally changed from control mice (Fig. 5C). The numbers of CD4$^+$ and CD8$^+$ naïve T cells (CD44^{low}CD62L^{high}) were significantly reduced in the Klf6^{KO} spleen (Fig. 5, A and B), whereas effector memory (CD44^{high}CD62L^{high}) and central memory (CD44^{high}CD62L^{low}) T cells were not altered (fig. S6, D and E). Homeostatic proliferation of conventional T cells and T_{reg} cells likely explains why the numbers of these T cell populations are minimally affected (*33*, *34*). In summary, naïve CD4$^+$ and CD8$^+$ T cell compartments in the spleen were specifically reduced.

Loss of CCL21$^+$CD104$^+$ mTEC^{lo} in TEC-specific *Ltbr* knockout mice resulted in a reduced proportion and cellularity of CD1d-restricted iNKT cells (*3*). Upon assessing iNKT cell populations in the thymus and spleen of Klf6^{KO} and Klf6^{WT}mice, we observed reduced fractions of iNKT cells among lymphocytes in 6- to 8-week-old mice (Fig. 5, D to F). Therefore, *Klf6* expression in TEC enhances iNKT cell development. Loss of CCL21$^+$ mTEC^{lo} is expected to result in the presence of self-reactive T cells in the periphery (*11*). To identify autoimmunity, we screened for lymphocytic infiltrates in Klf6^{KO} mice and age-matched controls at 9 months of age. None of the control mice exhibited lymphocytic infiltrates; however, all knockout mice showed dacryoadenitis of lacrimal glands and inflammation of their salivary glands (Fig. 5G). We also observed marked increases in anti-dsDNA autoantibodies in serum (Fig. 5H). Together, Klf6 deficiency in TEC reduced iNKT cell development and increased autoimmunity.

Klf6 modulates stages of maturation of CD4 thymocytes

We sought an explanation for the autoimmunity that was evident in Klf6^{KO} mice. No difference in the expression of TRAs, *Aire*, or *Fezf2* was observed in Klf6^{KO} mTEC II (fig. S6, F and G). Furthermore, mTEC I did not highly express Aire-independent TRA genes above baseline levels seen in other TEC such as cTEC, suggesting that the strong reduction of these cells and putative-associated TRAs is unlikely to contribute to signs of autoimmunity (fig. S6F). Previous work demonstrated that CCR7- or CCR7L-deficient mice have small numbers of SP thymocytes in the thymic cortex; the emigration of these cells without adequate medullary residence is thought to underlie the loss of central tolerance (*11*, *12*, *35*). Since conditional deficiency of *Klf6* markedly altered mTEC I and lowered *Ccl21a* gene expression, we assessed whether some CD4 SP thymocytes from Klf6^{KO} mice might similarly reside in thymic cortical sections using confocal microscopy. To clearly identify CD4 SP thymocytes, we used the expression of Thpok, which is a transcription factor expressed in CD4 lineage T cells after the double-positive (DP) stage, and required to impose the CD4 fate (*36*, *37*). We did not observe increases in the proportion of Thpok$^+$ thymocytes residing in the cortex of Klf6^{KO} mice compared with controls at steady state (fig. S7A). This remained the case after sublethal irradiation-mediated depletion of immature DP thymocytes (fig. S7B, top). Since inhibiting sphingosine-1-phosphate (S1P)–mediated lymphocyte egression enhanced the accumulation of mature thymocytes in the thymic cortex in CCR7- and CCR7L-deficient mice (*12*), we also treated Klf6^{KO} and Klf6^{WT} mice with FTY720. We observed no accumulation of Thpok$^+$ thymocytes in the thymic cortex of Klf6^{KO} compared with Klf6^{WT} mice after 10 days of being daily treated with FTY720 intraperitoneally (fig. S7B, bottom). These experiments indicate that *Klf6* deficiency in TEC does not prevent cortical-medullary migration as observed in CCR7- and CCR7L-deficient mice (*11*, *12*, *35*). Although defects in migration could remain below the threshold of detection of these experiments, we investigated whether additional mechanisms might help explain the autoimmunity evident in Klf6^{KO} mice.

To assess whether alterations in thymocyte development might be present in Klf6^{KO} mice, we cytometrically profiled developing thymocytes into stages of selection as previously described (fig. S7C) (*38*, *39*). We observed that CD4 SP thymocytes at the most mature stage undergoing negative selection, "wave 2b," were reduced in the Klf6^{KO} mice compared with Klf6^{WT} mice (Fig. 5I). Previous work that reported similarly reduced frequencies of CD4 SP Foxp3$^-$ Helios$^+$ thymocytes (*40*) also noted increased frequencies of CD4$^+$CD8^{low}Foxp3$^-$Helios$^+$ cells. Thus, we assessed whether similar alterations in TCR-dependent selection might be evident in thymocytes of Klf6^{KO} mice and found a similar increase in frequencies of CD4$^+$CD8^{low}Foxp3$^-$Helios$^+$ T cells (fig. S7D). Thus, our results suggest that potentially autoreactive clones could fail to be eliminated in the thymus of Klf6^{KO} mice, thus providing an explanation for the autoimmunity observed.

Klf6 favors a closed chromatin configuration in mTEC I

Klf6 is a DNA binding factor; thus, its removal would have both direct and indirect impacts on transcription. Klf6 also recruits several chromatin remodelers, including the histone deacetylase HDAC3 (*41*)—recently reported to induce mTEC development by repressing the cTEC transcriptional program (*42*). We hypothesized that loss of Klf6 induces chromatin accessibility changes in transcriptional regulatory regions, thus influencing gene expression. To test this hypothesis, sorted TEC from 4-week-old Klf6^{WT} and Klf6^{KO} mice were analyzed separately by scATAC-seq using the 10x Genomics platform. Datasets were processed using the Signac

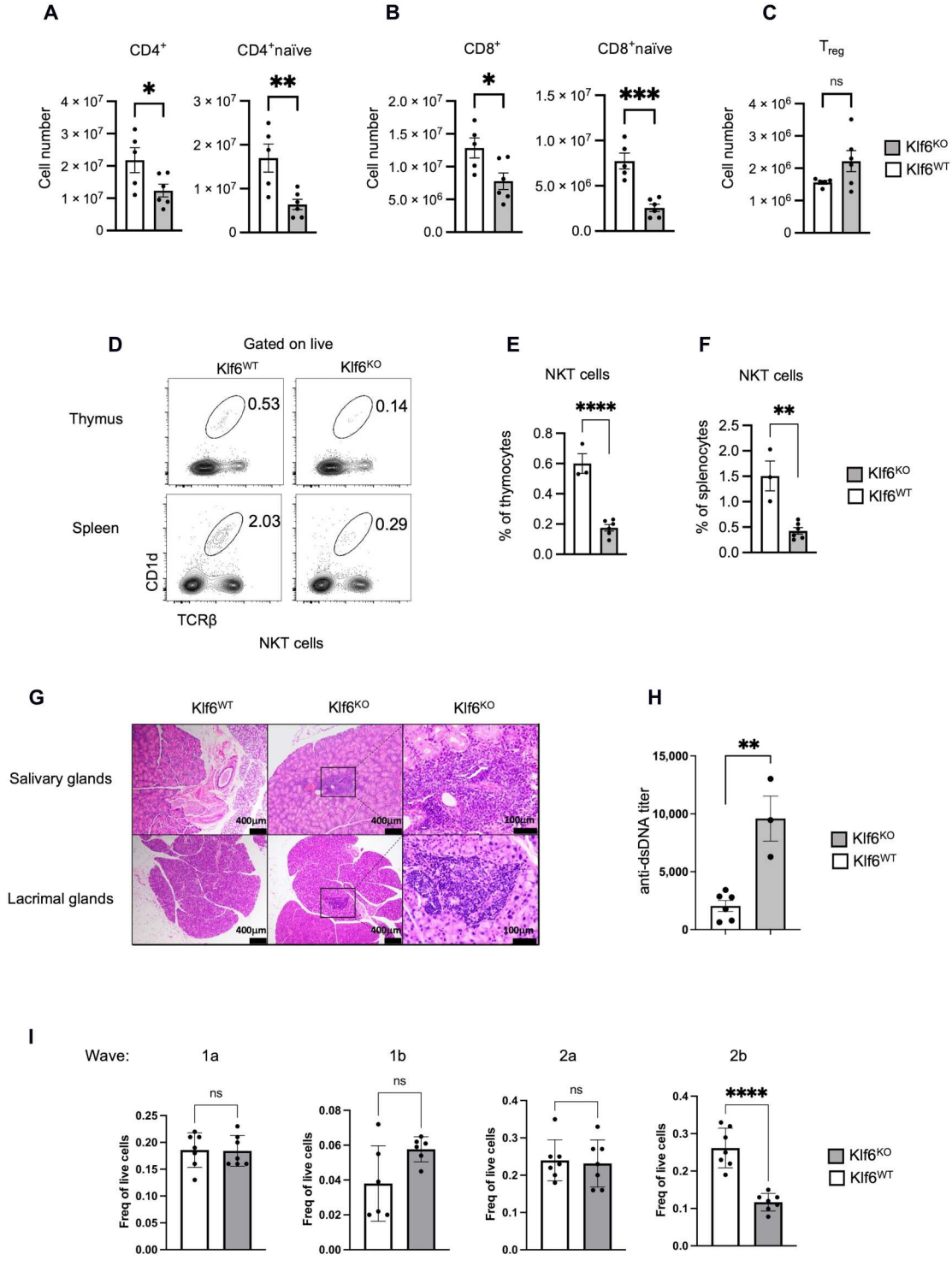

Fig. 5. Klf6^{KO} mice have alterations in peripheral T cell populations and increased markers of autoimmunity. (**A** to **C**) Barplots of cell counts for total CD4$^+$ T cells and naïve CD4$^+$ T cells (A), CD8$^+$ T cells and naïve CD8$^+$ T cells (B), and CD4$^+$ Foxp3$^+$ T$_{reg}$ cells (C) in spleens of Klf6^{WT} and Klf6^{KO} mice. (**D**) Representative flow cytometry plots of CD1d-tetramer$^+$TCRβ$^+$ cells in the thymus (top) and spleen (bottom) of Klf6^{KO} (right) and Klf6^{WT} (left) mice. (**E** and **F**) Barplots of the percentage of NKT cells in the thymus (E) and (F) spleen of Klf6^{KO} (right) and Klf6^{WT} (left) mice. (**G**) Hematoxylin and eosin staining of representative samples as indicated. Lymphocyte infiltration was noted in Klf6^{KO} tissues, with a higher magnification view of the indicated area shown on the right. In Klf6^{KO} mice, three out of three salivary glands and three out of three lacrimal glands exhibited infiltration, compared to zero out of three and zero out of three, respectively, in Klf6^{WT} mice. (**H**) Barplot of titers of anti-dsDNA (double-stranded DNA) autoantibodies detected in serum from Klf6^{WT} and Klf6^{KO} mice. (**I**) Frequency of live thymocytes at stages of negative selection as defined previously (*39*). Data were compiled from two independent experiments. Significance was computed using two-tailed unpaired Student's *t* tests. Error bars show ±1 SEM for a minimum of $n = 3$ mice per group. Data are representative of at least three independent experiments.

package (*43*) and cell clusters were annotated by transferring TEC labels from scRNA-seq datasets using the "gene activity" score from the scATAC-seq data (fig. S8A). There were no cells in the Klf6^{WT} data annotated as Sox10.

First, we assessed whether Klf6 ablation induced chromatin accessibility changes. Differentially accessible (DA) chromatin regions ("peaks") in Klf6^{KO} compared to Klf6^{WT} were identified for each TEC cluster (Fig. 6A). Klf6^{KO} TEC were enriched for DA peaks with greater accessibility compared to Klf6^{WT} with a particularly high proportion occurring in mTEC I (Fig. 6A), although with the caveat that a relatively small number of cells (*19*) was assigned as mTEC I in the Klf6^{KO} group and these cells were not clearly resolved from cTEC on the UMAP.

To expand our understanding of these DA peaks, we used Cicero (*44*), a platform that identifies putative spatially interacting co-accessible chromatin regions that function as cis-regulatory elements (*45*). "Positive co-accessibility" describes two chromatin regions with chromatin accessibility showing a direct proportional correlation across cells while "negative co-accessibility" refers to regions with inverse proportional correlation (schema in Fig. 6B). Negatively and positively co-accessible chromatin regions were significantly enriched in Klf6 motifs (Fig. 6B). Together with the markedly increased accessibility in mTEC I after Klf6 ablation (Fig. 6A), these observations suggest that Klf6 recruits chromatin remodelers in mTEC I that condense chromatin (fig. S8B). Supporting this, Klf6^{KO} mTEC I showed an ~2:1 ratio of up-regulated:down-regulated DEG that is significantly different from the ratio ~1:1 seen in all the remaining TEC subpopulations (fig. S8C). Overall, our results indicated that Klf6 likely represses chromatin accessibility and gene expression in mTEC I.

We next asked whether mTEC I DA peaks were closely associated with the DEG identified in our scRNA-seq datasets. When we examined the set of gene bodies (or, alternatively, transcriptional start sites) that directly flanked DA peaks, DEGs were no more

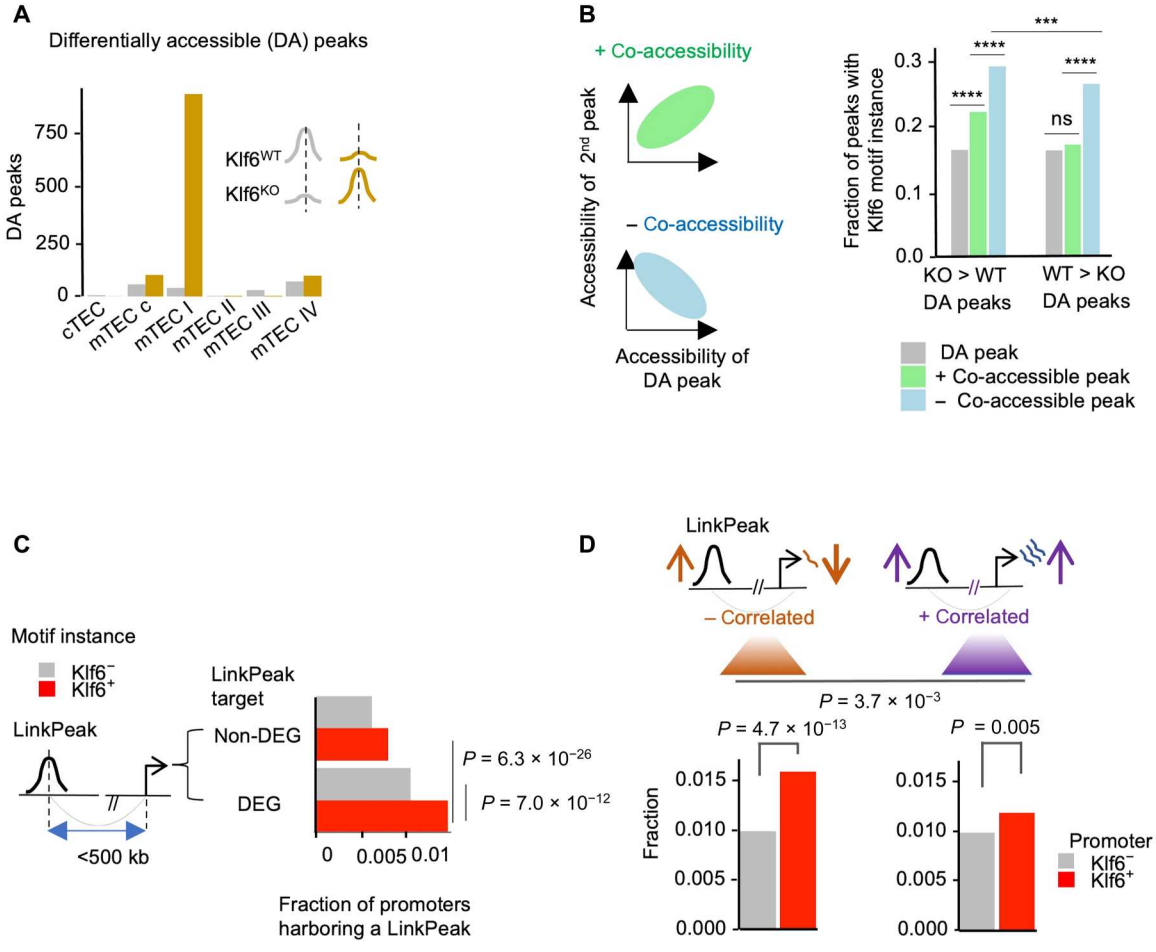

Fig. 6. Open chromatin peaks containing Klf6 motifs are enriched in DEGs up-regulated in Klf6^{KO}. (**A**) Differentially accessible (DA) chromatin peaks based on a minimum of fivefold higher fraction of cells with the open region and $P < 0.005$. (**B**) Left: Schematic representation of positive and negative co-accessibility between a DA peak and a second scATAC-seq peak, where co-accessibility is a proxy for spatial colocalization. Right: Bar chart showing fractions of chromatin peaks that harbor a Klf6 motif. Midpoints of open peaks ±250 bp were scanned for Klf6 motif instances. Co-accessible peaks were generated with the Cicero package. (**C**) Bar charts show the frequency of gene promoters with Linkpeaks, identified using Signac's "LinkPeaks" function, under indicated conditions. LinkPeaks were sorted by Klf6 motif presence and target gene classification. (**D**) Top: Schematic representation of negatively correlated LinkPeaks (left) as targeting DEG less highly expressed in Klf6^{WT} than Klf6^{KO} and positively correlated LinkPeaks (right) as targeting DEG more highly expressed in Klf6^{WT} than Klf6^{KO}. Bottom: Barplots of the fraction of gene promoters containing negatively correlated (left) and positively correlated (right), separated by the presence of a Klf6 motif.

enriched than among genes flanking random scATAC-seq peaks (fig. S8D). To computationally identify cis-regulatory elements targeting DEGs, we used the Signac function LinkPeaks (*46*), which scans for distal peaks ("LinkPeaks") whose accessibility is significantly correlated across cells with the expression of a putative target gene. We scanned all peaks less than 1500 base pairs (bp) upstream or 100 bp downstream of an accessible transcription start site (TSS) in each TEC population. We found that accessible promoters harboring a Klf6 motif ("Klf6$^+$ promoters") were substantially more likely to have a DEG target gene than Klf6$^-$ promoters (Fig. 6C). In addition, LinkPeaks targeting DEGs were enriched in Klf6$^+$ promoters relative to LinkPeaks targeting non-DEGs (Fig. 6C).

We further classified LinkPeak target gene pair relationships as either inductive—whereby LinkPeak accessibility is positively correlated with target gene expression across each Klf6^{WT} mTEC—or repressive, whereby peak accessibility and gene expression are negatively correlated (Fig. 6D). We found that open Klf6$^+$ promoters were enriched in both negatively and positively correlated LinkPeak-DEG pairs in mTEC (Fig. 6D); however, negatively correlated LinkPeak-DEG pairs are dominant relative to positively correlated LinkPeak-DEG pairs. Thus, accessible Klf6$^+$ promoters in each mTEC are more likely to be associated with repression of gene expression. Deficiency in *Klf6*, therefore, results in up-regulation of genes that are normally repressed.

In sum, Klf6 is imperative for establishing chromatin accessibility, particularly for closed chromatin, which enforces gene expression programs within mTEC subsets. These alterations are particularly notable in mTEC I, potentially explaining their stunted differentiation.

DISCUSSION

We report that TEC-specific loss of *Klf6* resulted in a hypoplastic thymus, including decreased thymocyte and TEC cellularity, from embryonic stages through adulthood. We identified that apoptotic- and stress-related pathways were up-regulated in embryonic and adult Klf6^{KO} TEC using scRNA-seq and verified these results using RT-qPCR and TUNEL staining. In adult mice, differentiation of mTEC I and, to a lesser extent, mTEC IV was greatly reduced in the Klf6^{KO} compared with Klf6^{WT}. Using scATAC-seq, we found that *Klf6* deficiency alters chromatin accessibility, especially in mTEC I. These TEC-specific alterations translated into alterations to the T cell compartment including reduced naïve conventional T cells and iNKT cells, as well as compromised central tolerance enforcement as demonstrated by lymphocyte infiltration in lacrimal and salivary glands and greatly increased titers of anti-dsDNA autoantibodies in aging (>9 months of age) mice.

Notably, a previously uncharacterized TEC population, expressing *Sox10* and *Epcam*, was evident in embryonic and adult scRNA-seq datasets after the integration of Klf6^{WT} with Klf6^{KO} TEC samples. We termed this cluster "Sox10 TEC" and verified its residency inside of the Ly51$^+$UEA1$^-$ cTEC compartment. scATAC-seq confirmed the statistical overrepresentation of Sox10 motifs within the cluster-specific open chromatin regions. Whereas Klf6^{WT} cells were present within the Sox10 cluster with Klf6^{KO} TEC, further research is needed to identify the prevalence of this cluster in wild-type mice and its role in thymus biology or T cell development.

The evident reduction of mTEC I and mTEC IV in the Klf6^{KO} mice was reminiscent of the phenotype observed after *Ltbr* ablation in TEC (*3*). Germline and TEC-specific *Ltbr*-deficient mice have impaired the development of mTEC expressing CCL21 but not of Aire$^+$ mTEC (*3*, *47*). The molecular drivers for mTEC I reduction in LTβR^{KO} mice have not been determined (*3*, *48*). It is considered that mTECc, characterized by their high expression of cell-cycling genes (*30*, *38*), give rise to the mTEC I and mTEC II populations (*30*). Therefore, we asked whether alterations in mTECc might explain the Klf6^{KO} mTEC I reduction. In the absence of mTECc-specific surface markers (*29*, *30*, *38*, *49*), we assessed proliferating TEC using in vivo BrdU labeling as a proxy. No reduction in the frequency of proliferating TEC was observed in Klf6^{KO} compared to Klf6^{WT} mice. Given that adult TEC progenitors are not well defined (*50*) and that putative progenitors of mTECc and other mTEC populations are consequently not known, we cannot rule out alterations in the proliferative capacity of an mTEC I–specific progenitor.

mTEC IV are regulated by the transcription factor Pou2f3 (*7*, *10*). In LTβR^{KO} mice, the remaining mTEC IV had lower Pou2f3 expression levels (*3*), whereas, in Klf6^{KO} mice, there was no change in the expression levels of Pou2f3 mRNA. mTEC IV can be generated along Aire-dependent and Aire-independent pathways with specific ablation of Aire$^+$ mTEC resulting in decreased post-Aire mTEC subsets (*8*, *51*), including mTEC IV (*10*). The mTEC IV Aire-independent developmental branch remains unexplored. Given that mTEC II and mTEC III were relatively unscathed in Klf6^{KO}, Klf6 might influence the Aire-independent mTEC IV developmental pathway, the life span of mTEC IV, or both.

Klf6 imposes gene silencing by recruiting chromatin-modifying proteins such as HDAC3 (*41*), a histone-modifying deacetylase enzyme that favors gene repression and chromatin compaction (*52*). *Foxn1*-mediated *Hdac3* ablation (Hdac3^{KO}) markedly affected all mTEC, including Aire$^+$ mTEC and their TRA gene expression (*42*). Therefore, some of the alterations in chromatin accessibility and gene expression observed in *Klf6*-deficient mTEC I may be due to the loss of Hdac3 function at those sites. Further research is needed to determine whether Klf6 interacts with additional chromatin-modifying complexes as do other members of the Klf family (*53*, *54*).

Germline LTβR-deficient mice exhibited massive lymphocyte infiltration in multiple organs (*55*, *56*) which was attributed to reduced expression of Fezf2 and its target genes rather than Aire-dependent TRA expression (which was unaltered) (*57*, *58*). Notably, TEC-specific deletion of *Ltbr* did not result in lymphocyte infiltration in any of the selected organs that were evaluated at 5 months of age (*48*)—perhaps due to normal expression levels of Fezf2 and Aire (*48*). Evidence of autoimmunity was discernable in Klf6^{KO} mice. However, no difference in the expression of TRAs, *Aire*, or *Fezf2* was observed in Klf6^{KO} mTEC II. Mice deficient in *Ccl21a* have defects in cortico-medullary migration of positively selected T cells, resulting in the retention of SP thymocytes in the cortex and the failed establishment of central tolerance (*35*). However, such increased cortical retention was not evident in our studies for CD4 SP cells, indicating that the remaining levels of Ccl21a were sufficient for migration from the cortex to the medulla. Instead, defects in the late stages of TCR-dependent selection of CD4 SP T cells were evident, as visualized by Helios up-regulation on late-stage CD4 SP Foxp3$^-$ thymocytes (*38*, *39*). The results could suggest that products of mTEC I may be important for SP T cells to scan for autoantigens in the medulla, but other models are also possible. Thus, products of mTEC I could be

required for efficient TCR signaling itself, or for retention of SP thymocytes to prevent their premature egress from the thymus into the periphery. Consistent with this last possibility, thymocytes from *Cd4-Cre Tgfbr2*$^{f/f}$ (TGFβR^{KO}) mice egressed prematurely from the thymus (*40*). TGFβR^{KO} and Klf6^{KO} mice share several features, such as increased frequencies of CD4^{+}CD8^{low}Foxp3^{-}Helios^{+} cells and correspondingly reduced frequencies of CD4 SP Foxp3^{-}Helios^{+} thymocytes, as well as autoimmunity. Further research is needed to uncover how mTEC lacking Klf6 fail to establish central tolerance.

In summary, conditional ablation of Klf6 affected TEC development by increasing cell death and altering the normal gene expression profile within TEC subsets. These alterations stunted the differentiation of specific mTEC subsets, particularly mTEC I. As a result, thymus function was compromised including the establishment of central tolerance, which appeared to occur by a pathway different from that seen in mice lacking Ccl21a itself. The results suggest that additional mechanisms remain to be found by which mTEC I act in self-tolerance induction. The identification and elucidation of these mechanisms will be the subject of future research.

MATERIALS AND METHODS

Mice

The *Klf6*-floxed (*Klf6fl/fl*) mice were obtained from Genentech (San Francisco, CA) (*17*). The *FoxN1Cre* mice were a gift from G. Hollander (*19*). *Klf6*-floxed mice were crossed with *FoxN1Cre* mice to generate an epithelial cell–specific deletion of *Klf6* (Klf6^{KO} mice). Mice described as newborns were 0 to 1 day (before ears appeared as nubs). Mice described as adults for flow cytometry/sequencing experiments were 4 to 6 weeks of age (unless otherwise stated). FTY20 (Sigma-Aldrich) resuspended in phosphate-buffered saline (PBS) was intraperitoneally administered to 6- to 8-week-old mice at the dose of 20 μg per day for 10 consecutive days (*12*). For irradiation experiments, 6- to 8-week-old mice were irradiated with a single dose of 450 rads (Gammacell 40 exactor, Best Theratronics Ltd). After 24 hours, the irradiated mice were euthanized, and thymi were analyzed (*35*). The ages of embryonic mice are specified with E0.5 being noon of the day post coitum evaluated as the vaginal plug in the female vagina after setting up a mouse breeding pair. Animal procedures were approved by relevant National Institutes of Health Animal Care and Use Committees.

Tissue preparation

The thymus and spleen were dissected into RPMI 1640 (Thermo Fisher Scientific) containing 5% fetal calf serum (Atlanta Biologicals), and 1× master mix (Pen-Srep, L-glutamine, amino acids, sodium pyruvate, and Hepes). Spleens were mechanically teased with forceps. Single-cell suspension was generated by gentling pipetting. To eliminate red blood cells, splenocytes were treated with ACK Lysing Buffer (Lonza) for 1 min on ice. After performing two washes in PBS, the splenocytes were stained as described below.

Embryonic and adult single-cell thymic suspensions were generated as previously described (*19*). Briefly, adult thymi were mechanically disrupted using surgical scissors. Single-cell thymic suspensions were generated by performing enzymatical digestions with Liberase TM Research Grade (63 μg/ml; Roche) and DNase I (20 μg/ml; Roche) for 40 min shaking at 37°C. Then, epithelial cells were taken from the interface between the Percoll and PBS layer after centrifugating the cells in a Percoll (GE) gradient. Embryonic thymi were enzymatically digested using 0.25% trypsin/0.02% EDTA (Sigma-Aldrich) solution at 37°C for 10 min. After this, single-cell suspension is made by gentle repetitive pipetting. Single-cell suspensions were then further processed and stained as described below.

Flow cytometry

Thymocytes and splenocytes were stained and analyzed in magnetic-activated cell sorting (MACS) buffer (PBS containing 2 mM EDTA and 0.5% fetal bovine serum). TEC preps were analyzed in MACS buffer. Antibodies specific for CD45.2 (104), Ly51 (6C3), EpCAM (G8.8), MHC class II (M5/114.15.2), CD80 (16-10A1), CD4 (GK1.5), CD8-α (53–6.72), TCRβ (H57), CD19 (1D3), CD44 (IM7), CD62L (MEL-14), CD25 (PC61.5), and streptavidin PECy7 were from eBioscience. Biotinylated UEA1 (B-1065) and FITC-UEA1 (B-1065) were from Vector Laboratories. CCL21 (59106) was from R&D Systems. DCLK1 (EPR6085) was acquired from Abcam. CD104 (346-11A), cleaved caspase-3 (C92-605), and BrdU (Kit, 552598) were acquired from BD Biosciences. CD117 (ACK2) was from BioLegend. CD1d tetramers were provided by the NIH Tetramer Facility. Viability discrimination was performed by staining with 4′,6-diamidino-2-phenylindole (DAPI; Sigma-Aldrich) for nonfixed cells or fixable blue dye from Thermo Fisher Scientific for fixed samples. For intracellular staining of CCL21, DCLK1, cleaved caspase-3, and BrdU, cells were first stained for cell surface molecules, fixed, permeabilized, and then either stained for specific antibodies. Experiments with CCL21, DCLK1, and BrdU used cells that were fixed and permeabilized using the FoxP3 staining kit (eBioscience) according to the manufacturer's instructions. Cleaved caspase-3 intracellular staining was accomplished using the BD Biosciences kit. All samples were acquired using a flow cytometer (LSRFortessa; BD Biosciences) and analyzed using FlowJo software (BD Biosciences). TEC were sorted using a BD FACSAria flow cytometer (BD Biosciences). The sorted cell purities were >98%. Cell numbers were counted using a CytoFLEX flow cytometer (Beckman Coulter). All TEC numbers were calculated from the frequency of CD45- EpCAM + cells of pre-enrichment samples.

Quantitative RT-PCR

Sorted cells were stored at −80°C until RNA was extracted using a Qiagen RNeasy Micro Extraction Kit. Reverse transcription was performed using the SuperScript VILO cDNA Synthesis Kit (Invitrogen). Quantitative PCR was performed on a StepOnePlus Real-Time PCR System (Applied Biosystems) using SYBR Green kit. Pmaip1 (forward 5′-TCAGGAAGATCGGAGACAAA-3′ and reverse 5′-TGAGCACACTCGTCCTTCAA-3′), Cdnk1a (forward 5′-TCCCGTGGACAGTGAGCAGTTG-3′ and reverse 5′-CGTCTCCGTGACGAAGTCAAAG-3′), Hprt (forward 5′-TTGCTCGAGATGTCATGAAGGA-3′ and reverse 5′-AGCAGGTCAGCAAAGAACTTATAG-3′). Results were analyzed using the ΔΔ cycle threshold method.

TUNEL and p63 staining

Whole embryos were dissected at the age of E15.5 and fixed in freshly prepared 4% paraformaldehyde (PFA) for 24 to 36 hours at room temperature and then processed into paraffin blocks.

Adult thymi were fixed in 4% PFA after the dissection. Five-micrometer sections were cut serially and mounted onto positively charged glass microscope slides. Slides were stained with the TUNEL kit and p63 antibody (D9L7L, Cell Signaling Technology) and DAPI. Slide images were acquired at a 20× magnification using an Aperio FL scanner.

Adult thymus immunofluorescence and H&E staining

Mouse tissues were harvested and fixed in 4% PFA (Thermo Fisher Scientific) and mounted in paraffin. Eight-micrometer sections were cut and stained with H&E (performed by Histoserv, MD). The evaluation of inflammatory cell infiltration in salivary and lacrimal glands was evaluated by an experienced pathologist following a single-blind scheme. Mouse thymus was harvested, embedded in Tissue-Tek OCT compound (Sakura Finetek), and flash-frozen. Ten-micrometer sections were cut using a cryotome and mounted on positively charged slides. Samples were fixed with 4% PFA and stained with H&E (performed by Histoserv, MD). The central sections were imaged using a Leica MZ12.5 microscope and a Nikon Coolpix 5000 camera. Cortical and medullary areas were quantified manually using ImageJ. For immunofluorescence, slides were washed with PBS, fixed with 4% PFA, and stained for Aire, Ccl21a [with Anti-Rabbit immunoglobulin G (IgG) secondary], UEA1 (Vector Laboratories, B-1065 or DL-1067-1), ThPok (BD Biosciences, T43-94), and DAPI. Images were acquired at a 20× magnification using tile imaging on a Nikon SoRa microscope.

BrdU staining

Pregnant mice were injected intraperitoneally (ip) with BrdU (1.5 mg) 18 hours before euthanasia, and embryonic thymi were processed as stated above. Four-week-old mice were injected intraperitoneally with BrdU (1.5 mg) and were euthanized after 14 hours. Cell suspensions were intracellularly stained for BrdU using the BD Biosciences APC BrdU Kit (552598), according to the manufacturer's instructions.

Simple Western

Klf6 protein expression was examined in mTEC using a Simple Western capillary electrophoresis system (R&D systems). Sorter mTEC were lysed with radioimmunoprecipitation assay. Simple Western was performed using automated capillary immunoassay system Peggy (ProteinSimple) according to the manufacturer's instructions. The primary and secondary Abs used for Simple Western are as follows: Klf6 monoclonal antibody (Santa Cruz Biotechnology, E10) and anti-mouse secondary HRP Ab (Simple Western, 042-205).

Enzyme-linked immunosorbent assay

Serum was obtained from Klf6^{WT} and Klf6^{KO} mice older than 9 months of age. Enzyme-linked immunosorbent assay (ELISA) for anti-dsDNA antibodies was performed with an ELISA kit (Thermo Fisher Scientific, 88-50400) according to the manufacturer's instructions. Briefly, diluted sera were applied to dsDNA-coated (10 μg/ml) 96-well plates. Primary antibody was detected with the horseradish peroxidase–conjugated anti-IgG secondary antibody (Thermo Fisher Scientific), followed by incubation with 3,3′,5,5′-tetramethylbenzidine substrate. After subtracting background values, titers were calculated as the greatest dilution to achieve an optical density of 0.1 at 450 nm.

Single-cell RNA sequencing

TEC were isolated by sorting from *Foxn1*$^{-}$*Cre*$^{-/-}$;*Klf6*$^{fl/fl}$ (Klf6^{WT}) or *Foxn1-Cre*$^{+}$;*Klf6*$^{fl/fl}$ (Klf6^{KO}) mice of 4 weeks of age by gating for CD45- EpCAM^{+} cells. To offset the difficulty in recovering cTEC from the digestion of adult thymus, additional cTEC were spiked into the Klf6^{WT} sample to achieve approximately equal numbers of cTEC and mTEC. cTEC and mTEC were sequenced as one sample on the 10x Chromium platform (10x Genomics), with separate runs performed for Klf6^{KO} and Klf6^{WT}. Regarding to eTEC, sorted TEC from E15.5 Klf6^{WT} and E15.5 Klf6^{KO} mice were sequenced separately. Libraries were constructed using the Chromium Single Cell 3′ Reagent Kits according to the manufacturer's instructions (v3 chemistry, 10x Genomics). Libraries were sequenced with a NextSeq 2k P2 (200 cycles). A primary analysis was performed with the Cell Ranger (version 5.0.1) software using the default parameters. Briefly, ~22,000 total genes were detected in ~2300 TEC per 4-week-old TEC sample, whereas ~9000 total genes in ~6000 cells per each eTEC sample. Single-cell analysis was performed using Seurat (version 4.1.0) applying default settings unless otherwise stated (*59*). It excluded cells with >10% mitochondrial gene content and >5000 genes per cell. The final integrated dataset used for analysis for 4-week-old mice included 1762 Klf6^{WT} and 1593 Klf6^{KO} TEC whereas for embryonic dataset included 3511 Klf6^{WT} and 4136 Klf6^{KO} E15 TEC. Mitochondrial content and cell cycle–related genes were regressed. It was performed UMAP dimensional reduction using principal components obtained from elbow plots. Cells were clustered using Seurat's FindClusters function. Contaminants were identified on the basis of gene expression signature determined using the function FindAllMarkers with a minimum $\log_2$ fold change threshold of 0.25 and the Wilcoxon rank sum test. After removing contaminant cells, the remaining cells were clustered again using Seurat's FindClusters function.

Analyses of single-cell RNA sequencing

Seurat's FindMarkers function was used to obtain the DEG between clusters considering those genes expressed in at least 10% of cells in the clusters to be compared. *P* values were determined using the Wilcoxon ranked sum test and genes with a Bonferroni-adjusted $P < 0.05$ are reported here. Violin plots shown in the figures were made using Seurat's normalized data. GO pathway analysis from specific DEG was carried out with the ClusterProfiler R package (version 4.0.5). Pseudo-time analyses were performed using the Monocle3 package applying default settings. The trajectory was manually initiated from mTECc.

Single-cell ATAC sequencing

Sorted TEC (CD45^{-}EpCAM^{+}) from Klf6^{WT} or Klf6^{KO} mice of 4 weeks of age were prepared. The cells were washed and lysed. According to the 10x ATAC user guide, ~500 nuclei of Klf6^{WT} and 2000 Klf6^{KO} were loaded and run into a Chromium instrument (10x Genomics) in separated lines. Libraries were sequenced with a NextSeq 500/550 High Output v2.5 (150 cycles). After that, the standard 10x Genomics Cell Ranger ATAC (version 1.2.0) pipeline was used to extract Fastqs, and the 10x Genomics Cell Ranger ATAC (version 1.2.0) pipeline was used to perform data processing. Sequenced reads were aligned to the 10x Genomics provided Mouse reference sequence. Approximately 4000 median fragments per cell for each TEC sample were detected. Integration of the datasets,

batch correction, UMAP dimension reduction, and clustering were performed using the Signac platform (*43*). The integrated dataset harbored 338 $Klf6^{WT}$ and 1670 $Klf6^{KO}$ single cells. To assign cell identity, for each cell in the scATAC-seq dataset, expression per gene was imputed via Signac's TransferData function, using the same principal components analysis (PCA) projection from scRNA-seq previously used for transferring TEC population labels to scATAC-seq.

Analyses of single-cell ATAC sequencing

Differentially accessible regions were determined using Signac's FindMarkers function with default parameters, except min.pct = 0.2. Differentially accessible peaks were those peaks that reached a $P < 5 \times 10^{-4}$ and absolute fivefold change difference in the cells exhibiting the peak. Klf6 cognate sites were called inaccessible regions using Bioconductor packages motifmatchr (max $P = 5 \times 10^{-5}$) and JASPAR2020.

Signac's LinkPeaks function was used to identify putative ATAC peak-target gene pairs. Cells were subsampled so that, for each TEC population, the sizes of $Klf6^{WT}$ and $Klf6^{KO}$ were that of the larger of $Klf6^{WT}$ and $Klf6^{KO}$. LinkPeaks parameters were set to defaults, except that min.cells was set to 5. The set of LinkPeaks for genes differentially expressed between $Klf6^{WT}$ and $Klf6^{KO}$ in each TEC population (Fig. 6, C and D) were found for the set of genes that, based on Seurat's FindMarkers, had $P < 0.005$, $|\log FC| > 0.1$, and $|pct_1 - pct_2| > 0.25$. For LinkPeak analysis, cell-specific gene expression was imputed via Signac's TransferData function based on the same PCA projection (default settings) used to transfer TEC population labels from scRNA-seq to scATAC-seq data (default setting). To enable comparison among populations and between negative and positive transcriptional regulators, filtered LinkPeaks were downsampled to 400 ensuring that LinkPeak sets for all populations and conditions were identical in size. The accessibility of each LinkPeak is significantly correlated with the expression of a nearby putative target gene (distance, <450 kb) across each TEC subpopulation. For promoters with a Klf6 motif ("$Klf6^{+}$ promoter"), the LinkPeak also must be $Klf6^{+}$. Promoters are defined as −1500:+100 bp around each TSS. Approximately 21,000 TSS were downloaded from Ensembl mm10. *P* values are computed using a one-sided Fisher's exact test.

The Cicero package (*44*) was used to impute population-specific spatial interactions between pairs of scATAC-seq peaks in each $Klf6^{WT}$ and $Klf6^{KO}$ TEC population. The number of interactions imputed is strongly affected by the number of cells analyzed. Therefore, to ensure populations were equally weighted, cells were downsampled in each population to 19, and the number of mTEC I was annotated in $Klf6^{KO}$ scATAC-seq data (all 16 $Klf6^{KO}$ mTEC IV were analyzed). Cicero parameters were adjusted to accommodate the sparser data (nDim = 9; F = 'approximate'; K = 6). For each TEC population, the top 50,000 positive co-accessible peak pairs and top 50,000 negative co-accessible peak pairs were culled on the basis of |corr|. Trends associated with Cicero interactions (Fig. 6B) were tested for robustness by, alternatively identifying population-specific interactions between scATAC-seq peaks based on default Cicero parameters and the full scATAC-seq dataset without downsampling.

Statistics

Tests of statistical significance were performed using GraphPad Prism. Differences between groups of samples were determined by an unpaired *t* test after testing that values fit the criteria for a normal distribution. If data did not fit a normal distribution, then a nonparametric Mann-Whitney test was used. $P < 0.05$ was considered statistically significant. $^{*}P < 0.05$, $^{**}P < 0.01$, $^{***}P < 0.001$, and $^{****}P < 0.0001$.

Supplementary Materials

This PDF file includes:
Figs. S1 to S8
Legends for tables S1 and S2
References

Other Supplementary Material for this manuscript includes the following:
Tables S1 and S2

REFERENCES AND NOTES

1. K. M. Ashby, K. A. Hogquist, A guide to thymic selection of T cells. *Nat. Rev. Immunol.* 10.1038/s41577-023-00911-8, (2023).
2. Y. Takahama, I. Ohigashi, S. Baik, G. Anderson, Generation of diversity in thymic epithelial cells. *Nat. Rev. Immunol.* **17**, 295–305 (2017).
3. B. Lucas, A. J. White, E. J. Cosway, S. M. Parnell, K. D. James, N. D. Jones, I. Ohigashi, Y. Takahama, W. E. Jenkinson, G. Anderson, Diversity in medullary thymic epithelial cells controls the activity and availability of iNKT cells. *Nat. Commun.* **11**, 2198 (2020).
4. S. W. Rossi, M. Y. Kim, A. Leibbrandt, S. M. Parnell, W. E. Jenkinson, S. H. Glanville, F. M. McConnell, H. S. Scott, J. M. Penninger, E. J. Jenkinson, P. J. Lane, G. Anderson, RANK signals from $CD4^{+}3^{-}$ inducer cells regulate development of Aire-expressing epithelial cells in the thymic medulla. *J. Exp. Med.* **204**, 1267–1272 (2007).
5. D. Gray, J. Abramson, C. Benoist, D. Mathis, Proliferative arrest and rapid turnover of thymic epithelial cells expressing Aire. *J. Exp. Med.* **204**, 2521–2528 (2007).
6. D. H. D. Gray, N. Seach, T. Ueno, M. K. Milton, A. Liston, A. M. Lew, C. C. Goodnow, R. L. Boyd, Developmental kinetics, turnover, and stimulatory capacity of thymic epithelial cells. *Blood* **108**, 3777–3785 (2006).
7. C. Bornstein, S. Nevo, A. Giladi, N. Kadouri, M. Pouzolles, F. Gerbe, E. David, A. Machado, A. Chuprin, B. Toth, O. Goldberg, S. Itzkovitz, N. Taylor, P. Jay, V. S. Zimmermann, J. Abramson, I. Amit, Single-cell mapping of the thymic stroma identifies IL-25-producing tuft epithelial cells. *Nature* **559**, 622–626 (2018).
8. D. A. Michelson, K. Hase, T. Kaisho, C. Benoist, D. Mathis, Thymic epithelial cells co-opt lineage-defining transcription factors to eliminate autoreactive T cells. *Cell* **185**, 2542–2558.e18 (2022).
9. J. L. Bautista, N. T. Cramer, C. N. Miller, J. Chavez, D. I. Berrios, L. E. Byrnes, J. Germino, V. Ntranos, J. B. Sneddon, T. D. Burt, J. M. Gardner, C. J. Ye, M. S. Anderson, A. V. Parent, Single-cell transcriptional profiling of human thymic stroma uncovers novel cellular heterogeneity in the thymic medulla. *Nat. Commun.* **12**, 1096 (2021).
10. C. N. Miller, I. Proekt, J. von Moltke, K. L. Wells, A. R. Rajpurkar, H. Wang, K. Rattay, I. S. Khan, T. C. Metzger, J. L. Pollack, A. C. Fries, W. W. Lwin, E. J. Wigton, A. V. Parent, B. Kyewski, D. J. Erle, K. A. Hogquist, L. M. Steinmetz, R. M. Locksley, M. S. Anderson, Thymic tuft cells promote an IL-4-enriched medulla and shape thymocyte development. *Nature* **559**, 627–631 (2018).
11. M. Kozai, Y. Kubo, T. Katakai, H. Kondo, H. Kiyonari, K. Schaeuble, S. A. Luther, N. Ishimaru, I. Ohigashi, Y. Takahama, Essential role of CCL21 in establishment of central self-tolerance in T cells. *J. Exp. Med.* **214**, 1925–1935 (2017).
12. H. Kurobe, C. Liu, T. Ueno, F. Saito, I. Ohigashi, N. Seach, R. Arakaki, Y. Hayashi, T. Kitagawa, M. Lipp, R. L. Boyd, Y. Takahama, CCR7-dependent cortex-to-medulla migration of positively selected thymocytes is essential for establishing central tolerance. *Immunity* **24**, 165–177 (2006).
13. B. B. McConnell, V. W. Yang, Mammalian Krüppel-like factors in health and diseases. *Physiol. Rev.* **90**, 1337–1381 (2010).
14. G. Narla, K. E. Heath, H. L. Reeves, D. Li, L. E. Giono, A. C. Kimmelman, M. J. Glucksman, J. Narla, F. J. Eng, A. M. Chan, A. C. Ferrari, J. A. Martignetti, S. L. Friedman, KLF6, a candidate tumor suppressor gene mutated in prostate cancer. *Science* **294**, 2563–2566 (2001).

15. K. Hu, Q. K. Zheng, R. J. Ma, C. Ma, Z. G. Sun, N. Zhang, Krüppel-like factor 6 splice variant 1: An oncogenic transcription factor involved in the progression of multiple malignant tumors. *Front. Cell Dev. Biol.* **9**, 661731 (2021).
16. N. Matsumoto, A. Kubo, H. Liu, K. Akita, F. Laub, F. Ramirez, G. Keller, S. L. Friedman, Developmental regulation of yolk sac hematopoiesis by Kruppel-like factor 6. *Blood* **107**, 1357–1365 (2006).
17. C. C. Leow, B.-E. Wang, J. Ross, S. M. Chan, J. Zha, R. A. Carano, G. Frantz, M. M. Shen, F. J. de Sauvage, W.-Q. Gao, Prostate-specific Klf6 inactivation impairs anterior prostate branching morphogenesis through increased activation of the Shh pathway. *J. Biol. Chem.* **284**, 21057–21065 (2009).
18. J. E. Cowan, J. Malin, Y. Zhao, M. O. Seedhom, C. Harly, I. Ohigashi, M. Kelly, Y. Takahama, J. W. Yewdell, M. Cam, A. Bhandoola, Myc controls a distinct transcriptional program in fetal thymic epithelial cells that determines thymus growth. *Nat. Commun.* **10**, 5498 (2019).
19. S. Zuklys, J. Gill, M. P. Keller, M. Hauri-Hohl, S. Zhanybekova, G. Balciunaite, K. J. Na, L. T. Jeker, K. Hafen, N. Tsukamoto, T. Amagai, M. M. Taketo, W. Krenger, G. A. Hollander, Stabilized β-catenin in thymic epithelial cells blocks thymus development and function. *J. Immunol.* **182**, 2997–3007 (2009).
20. M. Senoo, F. Pinto, C. P. Crum, F. McKeon, p63 Is essential for the proliferative potential of stem cells in stratified epithelia. *Cell* **129**, 523–536 (2007).
21. D. A. Zlotoff, A. Sambandam, T. D. Logan, J. J. Bell, B. A. Schwarz, A. Bhandoola, CCR7 and CCR9 together recruit hematopoietic progenitors to the adult thymus. *Blood* **115**, 1897–1905 (2010).
22. X. Tai, A. Indart, M. Rojano, J. Guo, N. Apenes, T. Kadakia, M. Craveiro, A. Alag, R. Etzensperger, M. E. Badr, F. Zhang, Z. Zhang, J. Mu, T. Guinter, A. Crossman, L. Granger, S. Sharrow, X. Zhou, A. Singer, How autoreactive thymocytes differentiate into regulatory versus effector $CD4^+$ T cells after avoiding clonal deletion. *Nat. Immunol.* **24**, 637–651 (2023).
23. E. M. Kernfeld, R. M. J. Genga, K. Neherin, M. E. Magaletta, P. Xu, R. Maehr, A single-cell transcriptomic atlas of thymus organogenesis resolves cell types and developmental maturation. *Immunity* **48**, 1258–1270.e6 (2018).
24. A. Karimian, Y. Ahmadi, B. Yousefi, Multiple functions of p21 in cell cycle, apoptosis and transcriptional regulation after DNA damage. *DNA Repair* **42**, 63–71 (2016).
25. E. Candi, A. Rufini, A. Terrinoni, A. Giamboi-Miraglia, A. M. Lena, R. Mantovani, R. Knight, G. Melino, ΔNp63 regulates thymic development through enhanced expression of FgfR2 and Jag2. *Proc. Natl. Acad. Sci. U.S.A.* **104**, 11999–12004 (2007).
26. L. Jeannotte, J. Aubin, S. Bourque, M. Lemieux, S. Montaron, A. Provencher St-Pierre, Unsuspected effects of a lung-specific Cre deleter mouse line. *Genesis* **49**, 152–159 (2011).
27. M. Irla, RANK signaling in the differentiation and regeneration of thymic epithelial cells. *Front. Immunol.* **11**, 623265 (2020).
28. T. Nitta, I. Ohigashi, Y. Nakagawa, Y. Takahama, Cytokine crosstalk for thymic medulla formation. *Curr. Opin. Immunol.* **23**, 190–197 (2011).
29. F. Dhalla, J. Baran-Gale, S. Maio, L. Chappell, G. A. Hollander, C. P. Ponting, Biologically indeterminate yet ordered promiscuous gene expression in single medullary thymic epithelial cells. *EMBO J.* **39**, e101828 (2020).
30. K. L. Wells, C. N. Miller, A. R. Gschwind, W. Wei, J. D. Phipps, M. S. Anderson, L. M. Steinmetz, Combined transient ablation and single-cell RNA-sequencing reveals the development of medullary thymic epithelial cells. *eLife* **9**, e60188 (2020).
31. Y. Aoki, N. Saint-Germain, M. Gyda, E. Magner-Fink, Y. H. Lee, C. Credidio, J. P. Saint-Jeannet, Sox10 regulates the development of neural crest-derived melanocytes in *Xenopus*. *Dev. Biol.* **259**, 19–33 (2003).
32. S. M. Muller, C. C. Stolt, G. Terszowski, C. Blum, T. Amagai, N. Kessaris, P. Iannarelli, W. D. Richardson, M. Wegner, H. R. Rodewald, Neural crest origin of perivascular mesenchyme in the adult thymus. *J. Immunol.* **180**, 5344–5351 (2008).
33. A. Liston, A. Y. Rudensky, Thymic development and peripheral homeostasis of regulatory T cells. *Curr. Opin. Immunol.* **19**, 176–185 (2007).
34. K. Takada, S. C. Jameson, Naive T cell homeostasis: From awareness of space to a sense of place. *Nat. Rev. Immunol.* **9**, 823–832 (2009).
35. T. Ueno, F. Saito, D. H. D. Gray, S. Kuse, K. Hieshima, H. Nakano, T. Kakiuchi, M. Lipp, R. L. Boyd, Y. Takahama, CCR7 signals are essential for cortex-medulla migration of developing thymocytes. *J. Exp. Med.* **200**, 493–505 (2004).
36. X. He, X. He, V. P. Dave, Y. Zhang, X. Hua, E. Nicolas, W. Xu, B. A. Roe, D. J. Kappes, The zinc finger transcription factor *Th-POK* regulates CD4 versus CD8 T-cell lineage commitment. *Nature* **433**, 826–833 (2005).
37. G. Sun, X. Liu, P. Mercado, S. R. Jenkinson, M. Kypriotou, L. Feigenbaum, P. Galéra, R. Bosselut, The zinc finger protein cKrox directs CD4 lineage differentiation during intrathymic T cell positive selection. *Nat. Immunol.* **6**, 373–381 (2005).
38. J. Baran-Gale, M. D. Morgan, S. Maio, F. Dhalla, I. Calvo-Asensio, M. E. Deadman, A. E. Handel, A. Maynard, S. Chen, F. Green, R. V. Sit, N. F. Neff, S. Darmanis, W. Tan, A. P. May, J. C. Marioni, C. P. Ponting, G. A. Hollander, Ageing compromises mouse thymus function and remodels epithelial cell differentiation. *eLife* **9**, e56221 (2020).
39. S. R. Daley, D. Y. Hu, C. C. Goodnow, Helios marks strongly autoreactive $CD4^+$ T cells in two major waves of thymic deletion distinguished by induction of PD-1 or NF-κB. *J. Exp. Med.* **210**, 269–285 (2013).
40. M. J. McCarron, M. Irla, A. Sergé, S. M. Soudja, J. C. Marie, Transforming growth factor-beta signaling in αβ thymocytes promotes negative selection. *Nat. Commun.* **10**, 5690 (2019).
41. D. Li, S. Yea, S. Li, Z. Chen, G. Narla, M. Banck, J. Laborda, S. Tan, J. M. Friedman, S. L. Friedman, M. J. Walsh, Krüppel-like factor-6 promotes preadipocyte differentiation through histone deacetylase 3-dependent repression of DLK1. *J. Biol. Chem.* **280**, 26941–26952 (2005).
42. Y. Goldfarb, N. Kadouri, B. Levi, A. Sela, Y. Herzig, R. N. Cohen, A. N. Hollenberg, J. Abramson, HDAC3 is a master regulator of mTEC development. *Cell Rep.* **15**, 651–665 (2016).
43. T. Stuart, A. Srivastava, S. Madad, C. A. Lareau, R. Satija, Single-cell chromatin state analysis with Signac. *Nat. Methods* **18**, 1333–1341 (2021).
44. H. A. Pliner, J. S. Packer, J. L. McFaline-Figueroa, D. A. Cusanovich, R. M. Daza, D. Aghamirzaie, S. Srivatsan, X. Qiu, D. Jackson, A. Minkina, A. C. Adey, F. J. Steemers, J. Shendure, C. Trapnell, Cicero predicts *cis*-regulatory DNA interactions from single-cell chromatin accessibility data. *Mol. Cell* **71**, 858–871.e8 (2018).
45. J. D. Buenrostro, B. Wu, U. M. Litzenburger, D. Ruff, M. L. Gonzales, M. P. Snyder, H. Y. Chang, W. J. Greenleaf, Single-cell chromatin accessibility reveals principles of regulatory variation. *Nature* **523**, 486–490 (2015).
46. S. Ma, B. Zhang, L. M. LaFave, A. S. Earl, Z. Chiang, Y. Hu, J. Ding, A. Brack, V. K. Kartha, T. Tay, T. Law, C. Lareau, Y. C. Hsu, A. Regev, J. D. Buenrostro, Chromatin potential identified by shared single-cell profiling of RNA and chromatin. *Cell* **183**, 1103–1116.e20 (2020).
47. E. Lkhagvasuren, M. Sakata, I. Ohigashi, Y. Takahama, Lymphotoxin β receptor regulates the development of CCL21-expressing subset of postnatal medullary thymic epithelial cells. *J. Immunol.* **190**, 5110–5117 (2013).
48. E. J. Cosway, B. Lucas, K. D. James, S. M. Parnell, M. Carvalho-Gaspar, A. J. White, A. V. Tumanov, W. E. Jenkinson, G. Anderson, Redefining thymus medulla specialization for central tolerance. *J. Exp. Med.* **214**, 3183–3195 (2017).
49. T. Miyao, M. Miyauchi, S. T. Kelly, T. W. Terooatea, T. Ishikawa, E. Oh, S. Hirai, K. Horie, Y. Takakura, H. Ohki, M. Hayama, Y. Maruyama, T. Seki, H. Ishii, H. Yabukami, M. Yoshida, A. Inoue, A. Sakaue-Sawano, A. Miyawaki, M. Muratani, A. Minoda, N. Akiyama, T. Akiyama, Integrative analysis of scRNA-seq and scATAC-seq revealed transit-amplifying thymic epithelial cells expressing autoimmune regulator. *eLife* **11**, e73998 (2022).
50. B. Lucas, A. J. White, F. Klein, C. Veiga-Villauriz, A. Handel, A. Bacon, E. J. Cosway, K. D. James, S. M. Parnell, I. Ohigashi, Y. Takahama, W. E. Jenkinson, G. A. Hollander, W. Y. Lu, G. Anderson, Embryonic $keratin19^+$ progenitors generate multiple functionally distinct progeny to maintain epithelial diversity in the adult thymus medulla. *Nat. Commun.* **14**, 2066 (2023).
51. T. C. Metzger, I. S. Khan, J. M. Gardner, M. L. Mouchess, K. P. Johannes, A. K. Krawisz, K. M. Skrzypczynska, M. S. Anderson, Lineage tracing and cell ablation identify a post-Aire-expressing thymic epithelial cell population. *Cell Rep.* **5**, 166–179 (2013).
52. L. Ning, X. Rui, W. Bo, G. Qing, The critical roles of histone deacetylase 3 in the pathogenesis of solid organ injury. *Cell Death Dis.* **12**, 734 (2021).
53. L. D. Boxer, B. Barajas, S. Tao, J. Zhang, P. A. Khavari, ZNF750 interacts with KLF4 and RCOR1, KDM1A, and CTBP1/2 chromatin regulators to repress epidermal progenitor genes and induce differentiation genes. *Genes Dev.* **28**, 2013–2026 (2014).
54. J. R. Moonen, J. Chappell, M. Shi, T. Shinohara, D. Li, M. R. Mumbach, F. Zhang, R. V. Nair, J. Nasser, D. H. Mai, S. Taylor, L. Wang, R. J. Metzger, H. Y. Chang, J. M. Engreitz, M. P. Snyder, M. Rabinovitch, KLF4 recruits SWI/SNF to increase chromatin accessibility and reprogram the endothelial enhancer landscape under laminar shear stress. *Nat. Commun.* **13**, 4941 (2022).
55. T. Boehm, S. Scheu, K. Pfeffer, C. C. Bleul, Thymic medullary epithelial cell differentiation, thymocyte emigration, and the control of autoimmunity require lympho-epithelial cross talk via LTbetaR. *J. Exp. Med.* **198**, 757–769 (2003).
56. A. Futterer, K. Mink, A. Luz, M. H. Kosco-Vilbois, K. Pfeffer, The lymphotoxin beta receptor controls organogenesis and affinity maturation in peripheral lymphoid tissues. *Immunity* **9**, 59–70 (1998).
57. E. S. Venanzi, D. H. D. Gray, C. Benoist, D. Mathis, Lymphotoxin pathway and Aire influences on thymic medullary epithelial cells are unconnected. *J. Immunol.* **179**, 5693–5700 (2007).
58. H. Takaba, Y. Morishita, Y. Tomofuji, L. Danks, T. Nitta, N. Komatsu, T. Kodama, H. Takayanagi, Fezf2 orchestrates a thymic program of self-antigen expression for immune tolerance. *Cell* **163**, 975–987 (2015).
59. Y. Hao, S. Hao, E. Andersen-Nissen, W. M. Mauck III, S. Zheng, A. Butler, M. J. Lee, A. J. Wilk, C. Darby, M. Zager, P. Hoffman, M. Stoeckius, E. Papalexi, E. P. Mimitou, J. Jain, A. Srivastava, T. Stuart, L. M. Fleming, B. Yeung, A. J. Rogers, J. M. McElrath, C. A. Blish, R. Gottardo,

P. Smibert, R. Satija, Integrated analysis of multimodal single-cell data. *Cell* **184**, 3573–3587.e29 (2021).

60. S. N. Sansom, N. Shikama-Dorn, S. Zhanybekova, G. Nusspaumer, I. C. Macaulay, M. E. Deadman, A. Heger, C. P. Ponting, G. A. Holländer, Population and single-cell genomics reveal the Aire dependency, relief from Polycomb silencing, and distribution of self-antigen expression in thymic epithelia. *Genome Res.* **24**, 1918–1931 (2014).

Acknowledgments: We thank the CCR Sequencing Facility and CCR Flow Cytometry Core Facility for technical support, B. Karim of the NCI Molecular Histopathology Laboratory, M. J. Kruhlak of the CCR Confocal Microscopy Core Facility, and X. Luo and R. Lake of the Microscopy Core for help with imaging. We thank S. Patel and R. Bosselut (NCI) for help with Thpok immunostaining, and V. S. Shapiro (Mayo Clinic, Minnesota) for reading the manuscript and providing comments. **Funding:** This work was supported by the Intramural Research Program of the National Cancer Institute, Center for Cancer Research, NIH. Support from the CCR Single Cell Analysis Facility was funded by FNLCR contract 75N91019D00024. G.U.M.-R. was supported by the National Council of Science and Technology (CONACyT-Mexico: CB A1-S-16997). **Author contributions:** Conceptualization: A.B. Methodology: Y.Z., G.U.M.-R., and S.C.S. Investigation: Y.Z., J.M., G.U.M.-R., S.C.S., J.E.C., A.M.-S., M.Ka., M.L., A.D., D.B., A.C.W., J.C., N.K., M.Ke., D.A., and L.R.B. Visualization: J.M., G.U.M.-R., Y.Z., and S.C.S. Supervision: A.B. Writing—original draft: J.M., G.U.M.-R., and Y.Z. Writing—review and editing: G.U.M.-R., Y.Z., S.C.S., J.M., A.B., all authors. **Competing interests:** The authors declare that they have no competing interests. **Data and materials availability:** All sequencing data have been uploaded to the Gene Expression Omnibus (https://ncbi.nlm.nih.gov/) under accession number GSE221074. All data needed to evaluate the conclusions in the paper are present in the paper and/or the Supplemental Materials.

Submitted 24 January 2023
Accepted 16 October 2023
Published 15 November 2023
10.1126/sciadv.adg8126